INFORMATION TO USERS

This manuscript has been reproduced from the microfilm master. UMI films the text directly from the original or copy submitted. Thus, some thesis and dissertation copies are in typewriter face, while others may be from any type of computer printer.

The quality of this reproduction is dependent upon the quality of the copy submitted. Broken or indistinct print, colored or poor quality illustrations and photographs, print bleedthrough, substandard margins, and improper alignment can adversely affect reproduction.

In the unlikely event that the author did not send UMI a complete manuscript and there are missing pages, these will be noted. Also, if unauthorized copyright material had to be removed, a note will indicate the deletion.

Oversize materials (e.g., maps, drawings, charts) are reproduced by sectioning the original, beginning at the upper left-hand corner and continuing from left to right in equal sections with small overlaps. Each original is also photographed in one exposure and is included in reduced form at the back of the book.

Photographs included in the original manuscript have been reproduced xerographically in this copy. Higher quality 6" x 9" black and white photographic prints are available for any photographs or illustrations appearing in this copy for an additional charge. Contact UMI directly to order.

UMI

A Bell & Howell Information Company
300 North Zeeb Road, Ann Arbor MI 48106-1346 USA
313/761-4700 800/521-0600

RECOMBINATION IN Kr^{34+} + H_2 AND O^{6+} + He COLLISIONS

by

Konstantinos Zaharakis

A Dissertation
Submitted to the
Fuculty of The Graduate College
in partial fulfillment of the
requirements for the
Degree of Doctor of Philosophy
Department of Physics

Western Michigan University
Kalamazoo, Michigan
December 1995

THE GRADUATE COLLEGE
WESTERN MICHIGAN UNIVERSITY
KALAMAZOO, MICHIGAN

Date November 9, 1995

WE HEREBY APPROVE THE DISSERTATION SUBMITTED BY

Konstantinos Zaharakis

ENTITLED Recombination in Kr^{34+} + H_2 and O^{6+} + He Collisions

AS PARTIAL FULFILLMENT OF THE REQUIREMENTS FOR THE

DEGREE OF Doctor of Philosophy

Physics
(Department)

John A. Tanis
Dissertation Review Committee Chair

Emanuel Y. Kamber
Dissertation Review Committee Member

Dan Heldman
Dissertation Review Committee Member

Gerald Hardie
Dissertation Review Committee Member

Maria Teresa Lee
Dissertation Review Committee Member

APPROVED

R. J. Douma
Dean of The Graduate College

Date December 1995

TABLE OF CONTENTS

LIST OF TABLES

LIST OF FIGURES

List of Figures - continued

List of Figures-continued

CHAPTER I

INTRODUCTION

A basic problem in atomic physics is the study of collisions of particles, and specifically collisions of projectile ions with neutral atoms. There are three major categories of events that occur in an ion-atom collision.[1]

1. Excitation: Electrons are excited from lower to higher energy states within the ion and, as a result, vacancies are produced in the energy levels originally occupied by the excited electrons.

2. Ionization: One or more electrons is lost from the ion or atom.

3. Charge transfer: Electrons from the neutral target are captured by the projectile ion (the target atom is ionized).

All three processes can be attributed to the Coulomb force between the interacting particles and therefore they are related. Each process takes place due to the interaction between the nucleus of one colliding partner and the electrons of the other, or between the electrons of the projectile ion and the electrons of the target atom. The distance between the interacting particles (i.e., the impact parameter), their charge, and the velocity at which

the collision takes place are the three factors that govern excitation, ionization and charge transfer. These processes can occur in either collision partner or in both, and it is important to note that combinations of these processes can occur as well.

Let us consider an ion-atom collision in which the combined process of electron capture by the ion and excitation of this same collision partner occurs. While any excitation is possible, we will consider only those excitations that give rise to K-shell vacancies, i.e., one or two electrons are promoted from $n = 1$ to $n \geq 2$ (n is the principal quantum number). The captured electron may occupy any unoccupied bound state of the ion. This charge-changed multi-excited state of the ion will subsequently decay by emitting either a photon(s) (x rays) or an electron(s) (Auger emission). Events which result in capture and K-shell excitation, yielding an intermediate multiply-excited state, and which subsequently decay by x-ray emission, are the primary emphasis of this thesis.

If the electron transfer is associated with a single K-shell electron excitation, an intermediate doubly-excited state is formed. In this case, there are three mechanisms by which this combined electron transfer and ion excitation can proceed. One is a two-step process called <u>non resonant transfer and excitation</u> (NTE)[2,3] in which the projectile is first excited through the Coulomb interaction with the

target nucleus (a projectile electron-target nucleus interaction) and subsequently captures an electron from the target (a target electron-projectile nucleus interaction). For NTE the excitation and capture events are independent.

If the combined process is due to the electron-electron interaction between an electron of the projectile and a (weakly bound) target electron, resonant formation of intermediate states can occur for specific incident ion velocities corresponding to Auger electron velocities (see Chapter II). In this process transfer and excitation take place simultaneously (i.e., it is a correlated process) and is called resonant transfer and excitation (RTE).[4]

The third mechanism by which this combined electron transfer and ion excitation can proceed is called two electron transfer and excitation (2eTE)[5] which is an uncorrelated process (i.e., capture and excitation are independent) as in the case of NTE. Here, however, the excitation is not due to an interaction with the captured electron as in RTE, or due to an interaction with the target nucleus as in NTE, but with a second target electron. Therefore, in 2eTE excitation and capture are not correlated and no resonant behavior is expected.

RTE is analogous to the fundamental ion-electron recombination process referred as dielectronic recombination[6] (DR). The only difference between RTE and DR is that in RTE the captured electron is initially bound in

an atom while in DR the captured electron is free. Both processes lead to the same intermediate excited states.

DR is of considerable interest in astrophysical studies[7], accelerator development (storage rings), and high-temperature plasmas for fusion.[8] During the last decade RTE has been studied extensively, and today the close relationship between RTE and DR is clearly established. Therefore, in addition to its fundamental importance as a correlated two-electron process in ion atom collisions, RTE has been of considerable applied interest since it provides a means of studying DR. Until recently, laboratory measurements of DR were difficult because of the difficulties of using free electrons as a target. Hence, RTE measurements have provided much useful data for the testing of DR calculations.[4]

The principal mechanism investigated in this work, namely, resonant electron transfer and double excitation (RT2E), is similar to RTE except that two inner-shell electrons are excited during the capture process. RT2E is expected to occur resonantly via a correlated three-electron interaction, and the intermediate excited state that is formed can subsequently decay by photon or Auger emission.[9] As for RTE, in the case of x-ray emission, the signature for RT2E is detection of this photon in coincidence with a projectile that has captured an electron. RT2E can be distinguished from RTE, however, since the resonant

energies for RT2E are about twice those for RTE. A process analogous to RT2E has been observed[10] in collisions of free electrons with Li^+ ions; in this work the intermediate triply-excited state which was formed as a result of the single capture double-excitation process was observed from decay occurring by the emission of two correlated electrons. The inverse of the RT2E process, involving double inner-shell de-excitation associated with the emission of a single electron, was seen[11] several years ago. Competing with this latter process is double decay accompanied by single photon emission.[12] The study of such correlated multielectron transitions dates back to the early days of the quantum theory of atoms.[13]

The main emphasis of this thesis is to present experimental work that has been done to investigate the proposed mechanism of RT2E in collisions of Kr^{34+} and O^{q+} (q=5,6) ions with H_2 and He targets respectively. As a benchmark for RT2E, measurements for RTE were also made. Additionally, radiative electron capture[14] (REC), involving single electron capture accompanied by simultaneous x-ray emission (i.e., inverse of the photoelectric effect), was investigated.

CHAPTER II

THEORETICAL CONSIDERATIONS

In the collision between a projectile ion and a neutral target atom, ion excitation and electron capture from the target can occur together, in a single encounter, resulting in the formation of an intermediate doubly excited state. This intermediate excited state decays by either photon (x-ray) emission or electron (Auger) emission. These reactions can be expressed by the notation:

$$A^{q+} + B \rightarrow [A^{(q-1)+}]^{**} + B^{+} \qquad (2.1)$$
$$\hookrightarrow \begin{cases} A^{(q-1)+} + h\nu \\ A^{q+} + e^{-} \end{cases}$$

For a Li-like (i.e., three-electron) ion, these reactions are shown schematically in Figure 1.

Electron emission occurs in the de-excitation of the intermediate state when one electron falls to the K-shell without the emission of radiation. The ejected electron is called an Auger electron and its kinetic energy (K) depends upon its binding energy E_n before emission and upon the energy difference between the excited and ground states of the ion, ΔE, i.e., $K = \Delta E - E_n$.

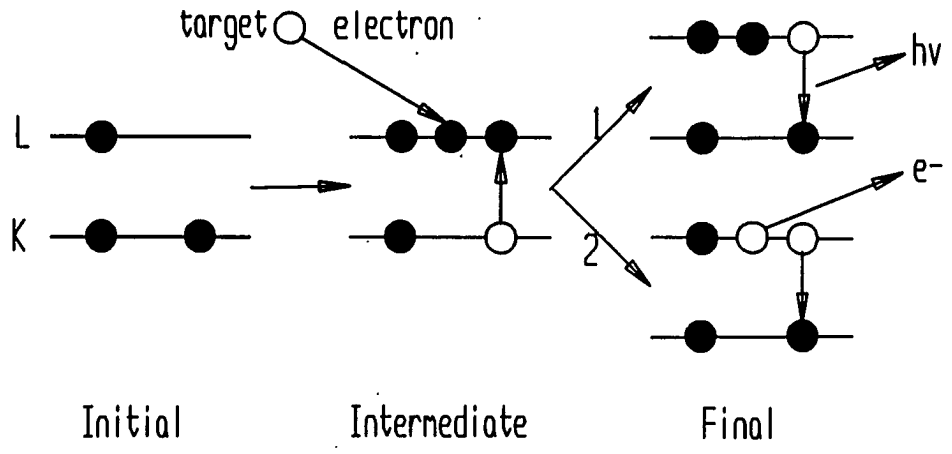

Figure 1. Schematic Showing the Initial, Intermediate, and Final States of a Li-Like Ion Undergoing Combined Capture and Excitation When Colliding With a Target Atom.

It should be noted that ΔE is the difference in energy between the initial and final states which are in two different ions since the charge state increases with Auger emission. Since electrons that are bound in an ion obey quantization rules, ΔE and E_n have discrete values so K has discrete values also. Therefore, the energy of the Auger electron is a well-defined quantity for any particular Auger emission. In the Auger process, de-excitation and electron emission are events that take place simultaneously due to the electron-electron interaction.

The processes of interest here, namely DR, RTE, and RT2E, take place via the time-reversed Auger mechanism. A schematic of the formation of the intermediate state in the dielectronic recombination process is shown in Figure 2,

where the "wavy" line represents the interaction which takes place. By definition, subsequent emission of the de-excitation photon is part of the DR process.

Comparing Figures 1 and 2, we can see that DR proceeds through the time-reversed Auger process. It was mentioned before that the kinetic energy of the Auger electron has only discrete values, and since DR is the time-reversed Auger process, it too depends upon the energy difference between the initial and final states of the projectile ion. This means that, in the rest frame of the ion, the energy of the colliding electron must equal the corresponding Auger energy for the transition to take place. Therefore, resonance conditions in DR occur when the relative velocity of the projectile ion and the target electron is equal to to the velocity of the Auger electron that would be ejected as a result of the decay of the doubly-excited state of the ion. The principal difference between DR and RTE is that for the latter process the captured electron is initially (weakly) bound in a target. Theoretical calculations of DR cross sections have been done[15,16,17] during the last years and these cross sections, together with the momentum distribution of the target atoms (see below), are used in the theoretical calculations of the RTE cross sections.

A process which competes with RTE (i.e., it gives rise to the same intermediate states) is nonresonant transfer and excitation (NTE). A schematic of the NTE process is

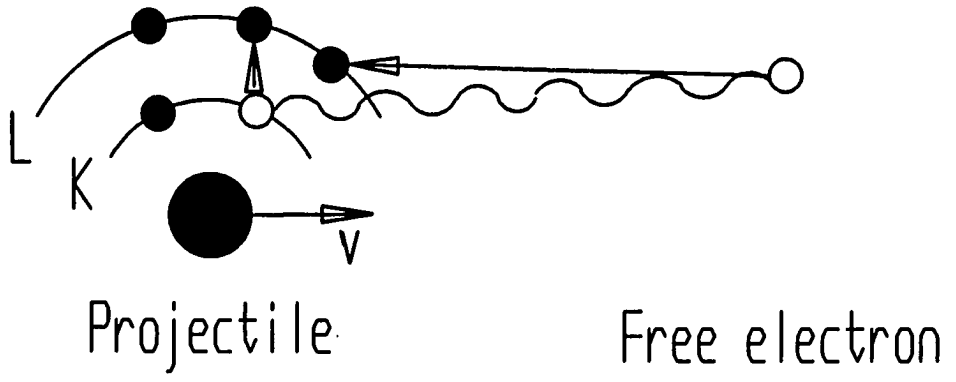

Figure 2. Schematic Showing Formation of the Doubly-Excited Intermediate Resonant State in Dielectronic Recombination for a Li-Like Ion Colliding With a Free Electron.

shown in Figure 3, again for a Li-like ion with the "wavy" lines representing the interactions. Referring to this figure we see that NTE is a two-step process; the formation of the intermediate excited state occurs first by excitation of a projectile electron through the Coulomb interaction with the target nucleus, and, second, by capturing an electron from the target atom. The capture and excitation events are independent and therefore no resonant conditions are involved in NTE.

Since NTE is a two-step process (excitation followed by capture) the NTE cross section depends on both the excitation and capture probabilities. Mathematically the NTE cross section is given by the expression:[2,3]

$$\sigma_{NTE} = \int_0^\infty 2\pi P_K^{ex}(b)\, P_L^{cap}(b)\, b\,db \qquad (2.2)$$

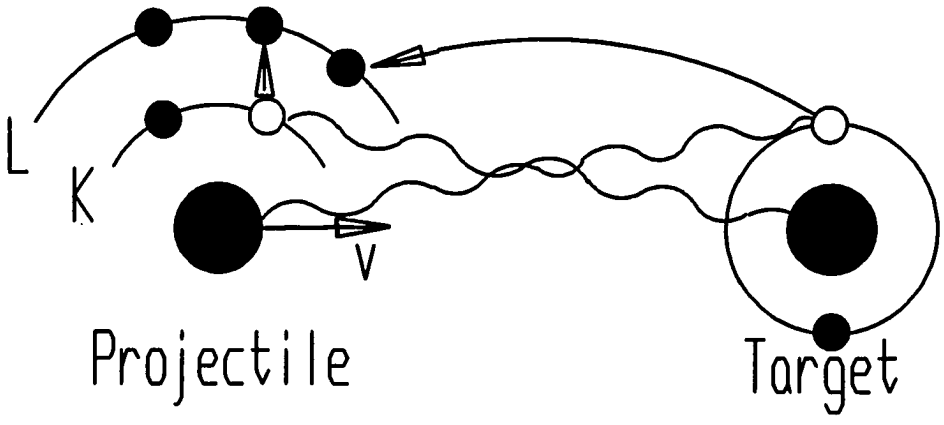

Figure 3. Schematic of the NTE Process for a Li-Like Ion.

where b is the collisional impact parameter, $P_K^{ex}(b)$ is the K-shell excitation probability of the ion, and $P_L^{cap}(b)$ is the capture probability of a target electron to the L shell of the ion. Over the range of b where $P_K^{ex}(b)$ is nonzero, $P_L^{cap}(b)$ is expected to be approximately constant[2,3] and equal to $P_L^{cap}(0)$ (i.e., the probability for zero impact parameter).

Therefore,

$$\sigma_{NTE} = 2\pi P_L^{cap}(0) \int_0^\infty P_K^{ex}(b)\, b db \qquad (2.3)$$

Since

$$\sigma_K^{ex} = 2\pi \int_0^\infty P_K^{ex}(b)\, b db \qquad (2.4)$$

the former expression becomes

$$\sigma_{NTE} = P_L^{cap}(0) \cdot \sigma_K^{ex} \qquad (2.5)$$

In Figure 4, the qualitative behaviors of $P_L^{cap}(0)$, σ_K^{ex}, and σ_{NTE} are shown schematically. Thus, the NTE cross sections can be predicted from the product of the K-shell excitation cross section and the probability for electron capture to the L-shell at small impact parameters (near zero).

The projectile energy where the maximum NTE cross section occurs will vary depending upon the charge state of the projectile and upon the atomic number of the target. NTE is generally expected to be dominant at projectile energies lower than those for which RTE occurs.[18,19,20,21]

A final process which competes with RTE is two electron transfer and excitation (2eTE). A schematic of the 2eTE process is shown in Figure 5. Referring to this figure, we see that 2eTE is also a two-step process, like NTE, but here the excitation is not due to the interaction with the target nucleus but due to the interaction with a second target electron. To date, there are no accurate numerical calculations available for 2eTE cross sections. Rough estimates of 2eTE cross sections[5] are made using calculated cross sections for excitation by free electrons[22] and Oppenheimer-Brinkman-Kramers capture probabilities.[5]

Let us now focus on RTE itself which, as already ment-

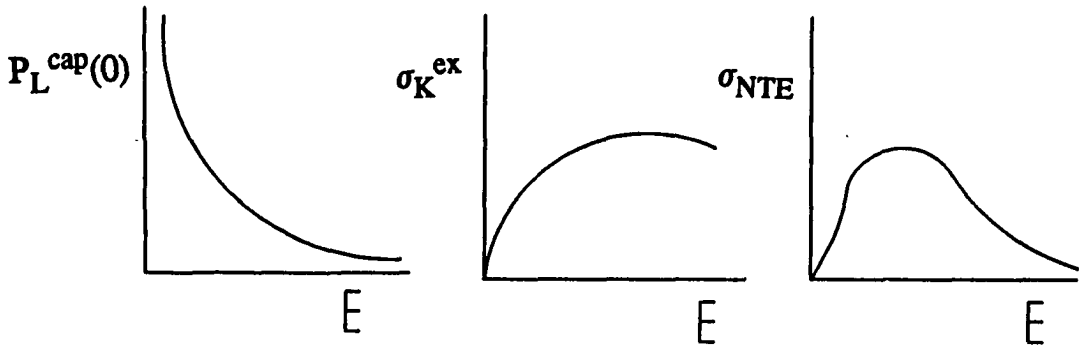

Figure 4. Schematic of the NTE Cross Section σ_{NTE} as a Product of the L-Shell Capture Probability $P_L^{cap}(0)$ (for Small Impact Parameters), and the K-Shell Excitation Cross Section, σ_K^{ex}.

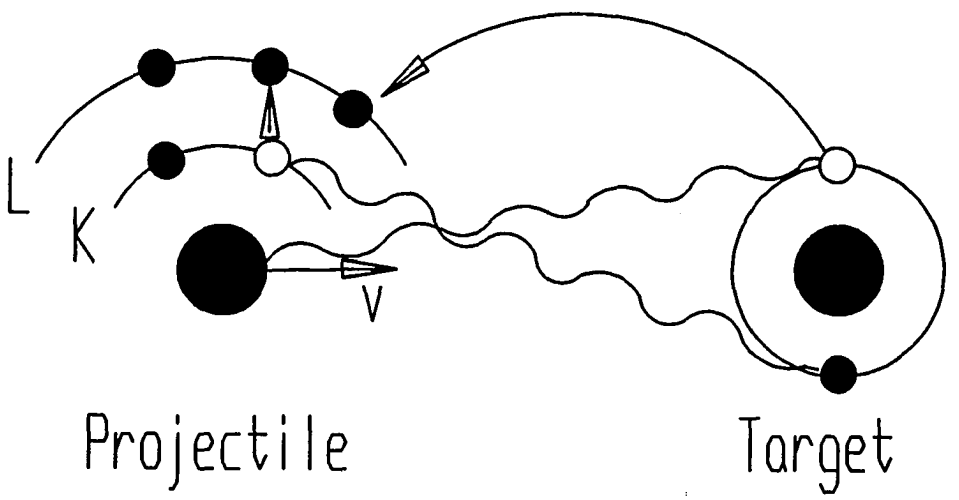

Figure 5. Schematic of the 2eTE Process for a Li-Like Ion.

ioned is very similar to DR. RTE occurs in an ion-atom collision when excitation of the ion is accompanied by capture of a target electron. Subsequent relaxation by x-ray emission results in recombination (analogous to DR) while relaxation by Auger emission returns the ion to its

original charge state. It is important to note that the excitation and capture occur (see Figure 1) only when the relative velocity of the projectile ion and the captured electron, for the particular resonance state formed, matches the velocity of the ejected Auger electron in the inverse process. Referring to Figures 1 and 2, we can see that the only difference between RTE and DR is the initial state of the target electron, i.e., for RTE the electron is bound, while for DR the electron is free.

The theoretical formulation[23] of RTE is based on the impulse approximation, which assumes that immediately after the collision the separation between the projectile and target is such that no further interaction takes place. In order to satisfy the impulse approximation, the velocity of the ion must be much greater than the velocity of the captured target electron (i.e., $V_{ion} >> V_{electron}$). The RTE velocities for the systems considered here (on the order of projectile K-shell electron velocities) satisfy this criterion for the weakly bound electrons of H_2 or He targets. Therefore, the theoretical interpretation of RTE is given by approximating the ion-atom collision as a collision between an ion and a free electron. Of course, many intermediate resonance states are possible in the RTE process, but here we focus only on those transitions in which at least one of the active electrons involved in the RTE process occupies a level in the intermediate state with

principal quantum number n = 2 (i.e., a K-shell electron of the projectile is promoted to the L-shell simultaneous with the capture of a target electron to n ≥ 2).

In the impulse approximation, RTE is equivalent to dielectronic recombination averaged over the electron momentum distribution of the target electrons, so the cross section is given by:

$$\sigma_{RTE} \sim \sigma_{DR} \sum_i J_i(p_{iz}) \qquad (2.6)$$

where σ_{RTE} is the RTE cross section, σ_{DR} is the DR cross section and $J_i(p_{iz})$ is the Compton profile (momentum distribution) of the target electron (i.e., the probability of finding a particular target electron with momentum component p_{iz} along the beam axis). As noted earlier, DR cross sections for several ions have been calculated to date.[15,16,17] In this thesis, the RTE measurements presented are compared with calculations based on Equation (2.6).

The Compton profile term results from the fact that the electrons available for capture are bound to the nucleus of the target atom. Compton profiles of all atoms have been tabulated[24] from numerical calculations based on Hartree-Fock wave functions. The Compton profile for the electrons in a neutral, ground state atom is a symmetric bell-shaped function of momentum, p, centered about p=0. A graphical representation of the Compton profile for H_2 is

shown in Figure 6, where $J_i(p_{iz})$ is the probability momentum distribution function of the target electron and P_{iz} is the z component of the momentum of the i^{th} electron in the target. In Equation (2.6), the Compton profile is summed over all electrons which can contribute to the formation of the specific intermediate state.

Referring to Figure 6 we can see that in the laboratory rest frame the target electron is most likely to have a zero momentum component along the beam axis (z axis). In addition, the Compton profile for the electrons in any given atom is a continuous function of momentum. Therefore, a range of relative velocities between the projectile and the target electron satisfy the resonance condition (i.e., equal to the Auger electron velocity), and intermediate resonance states corresponding to RTE can be formed over this range. Since these states are identical to the resonance states of DR, the Compton profile term in Equation (2.6) broadens the relatively narrow DR peaks corresponding to the particular resonance states. The extent to which the peak is broadened is proportional to the width of the Compton profile.

In the rest frame of the ion, the momentum of the i^{th} electron along the beam axis is given by:[23]

$$P_{iz} = \left(K - \frac{Em}{M}\right)\left(\frac{M}{2E}\right)^{1/2} \qquad (2.7)$$

where K is the corresponding Auger energy for the (interme

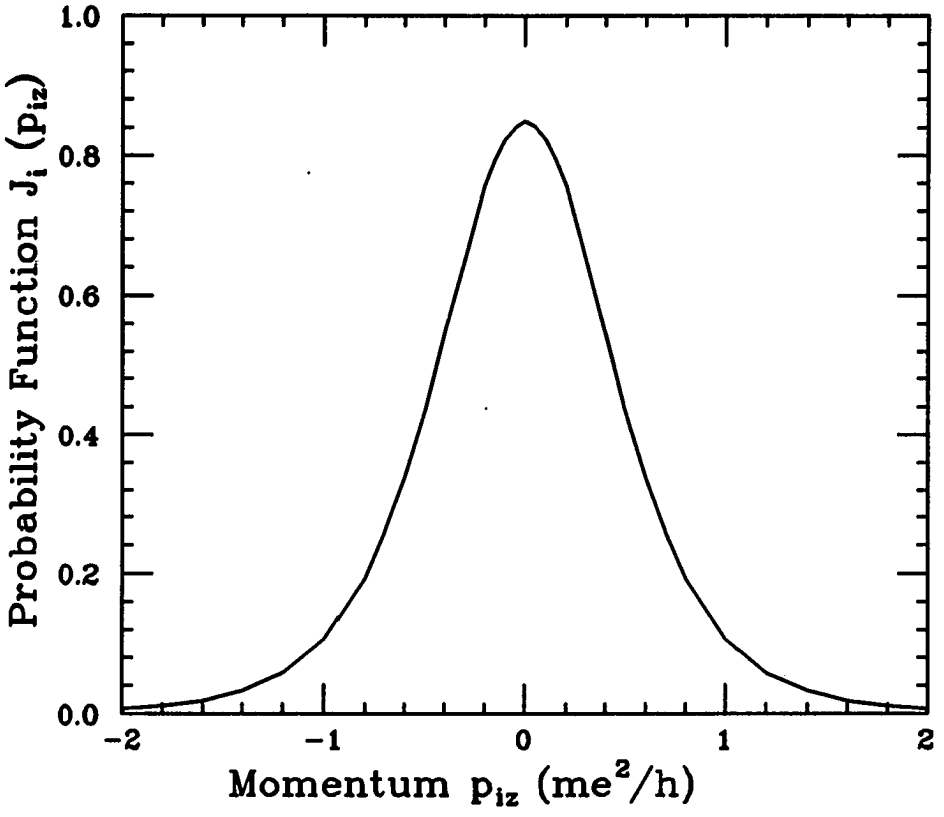

Figure 6. Graphical Representation of the Compton Profile for H_2.

diate-state) transition that takes place, E is the projectile energy, m is the mass of the electron and M is the mass of the projectile ion.

For $P_{iz} = 0$ (the Compton profile has its maximum at $P_{iz} = 0$) Equation (2.7) implies that:

$$E = \frac{KM}{m} \qquad (2.8)$$

Equation (2.8) simply transforms the position of each

broadened peak from the Auger energy to the laboratory frame projectile energy.

We can now summarize the effect of Equation (2.6) by saying that a DR resonance is broadened by having the target Compton profile superimposed upon it, and then transformed to the projectile lab frame energy. This is done for each of the DR peaks representing different intermediate excited states. The contributions due to each peak are added together to obtain the total RTE cross section. For the Kr^{34+} + H_2 system investigated here the maximum RTE cross section calculated[9] from Equation 2.6 for KLL transitions is 1.2×10^{-21} cm^2. (The notation KLL means single excitation to the L-shell is accompanied by capture to the L-shell).

The primary mechanism investigated in this work, namely, resonant-transfer-double excitation (RT2E), is similar to RTE except that two inner-shell electrons are excited during the capture process. Both mechanisms are illustrated schematically for a heliumlike ion in Figure 7. A theoretical estimate[9] of the maximum RT2E cross section for K^{34+} + H_2 KKLLL transitions (the notation KKLLL means double excitation to the L-shell is accompanied by capture to the L-shell) involving radiative stabilization by two sequential photons, gives about 10^{-27} cm^2, while the RT2E cross section for one photon followed by Auger emission (or vice versa) is about 10^{-28} cm^2. For both estimates the

theoretical uncertainty is on the order of a factor of 10.

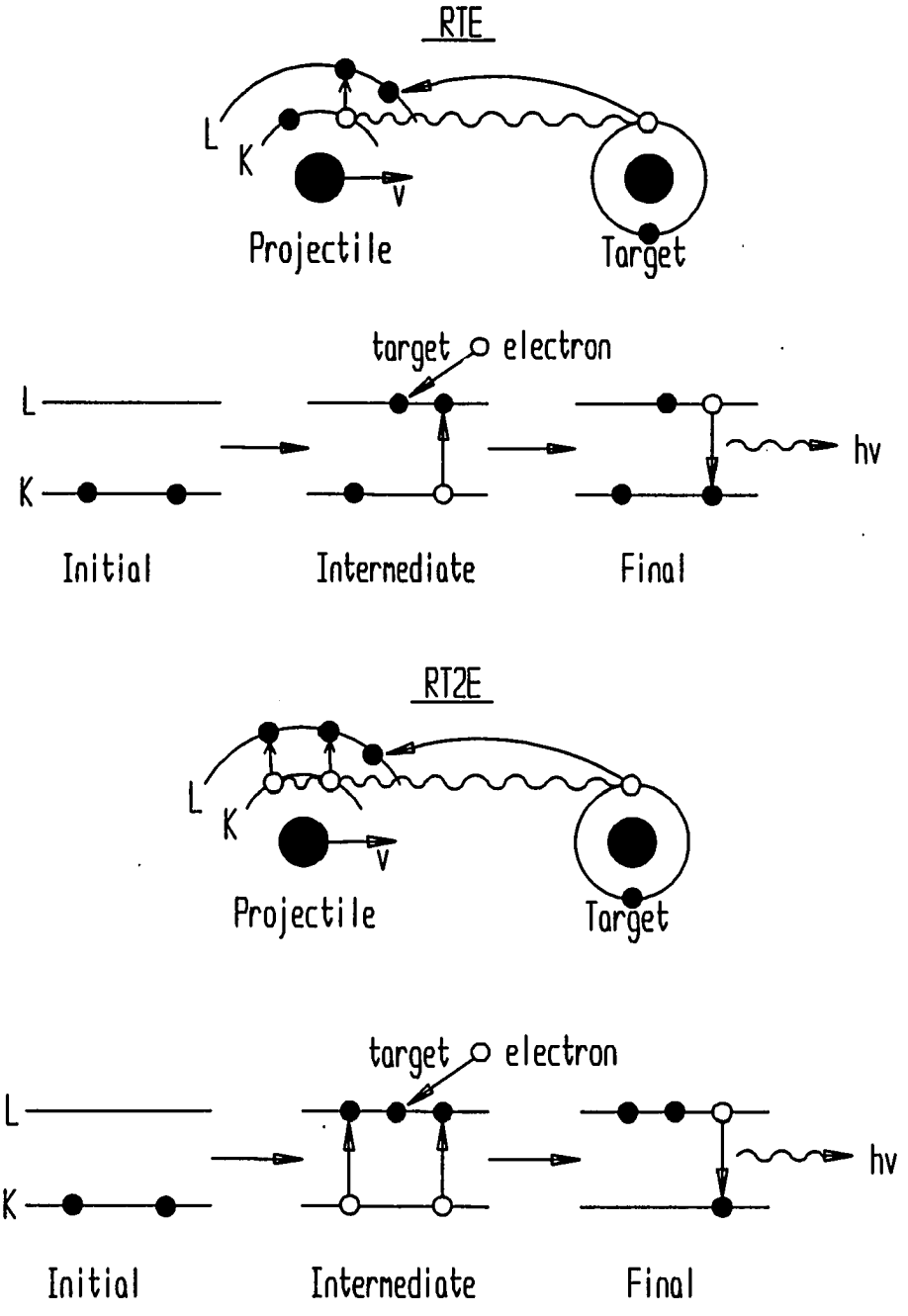

Figure 7. Schematic of RTE and RT2E for a Heliumlike Ion.

The calculated cross section profiles for RTE and RT2E (assuming sequential photon emission) for Kr^{34+} + H_2 are shown in Figure 8 as a function of the projectile beam energy. The Auger notation on each peak indicates the electronic transition that takes place during the collision.

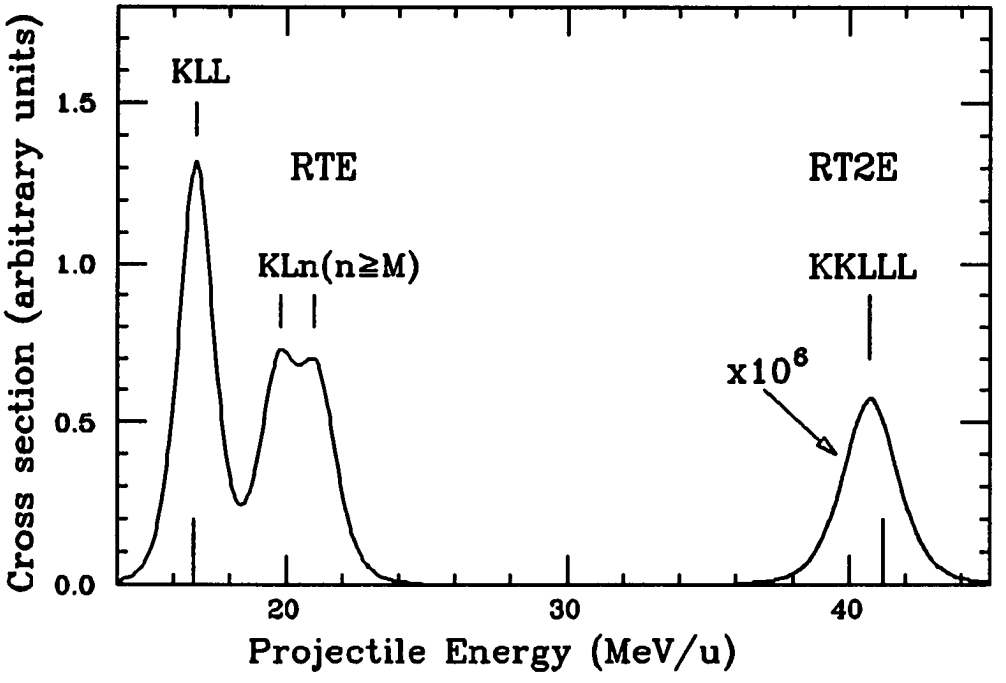

Figure 8. Calculated Cross Section Profile of RTE and RT2E for Kr^{34+} + H_2

The reaction energy for any particular RTE or RT2E transition is calculated by taking the difference in total binding energies between the initial and intermediate states of the projectile ion (see Figure 7). For example, the total binding energy of Kr^{34+} in the $1s^2$ ground state is equal[25] to -35.230 keV, while the 1s2s2p excited state

has total binding energy equal[25] to -26.400 keV. Therefore, the reaction energy for this particular RTE transition (KLL), in the rest frame of the ion, is equal to 8.83 keV. However, in order to calculate the reaction energy in the laboratory frame, one has to use equation 2.8 where K=8.83 keV and M/m = 1823/u. Thus, the necessary amount of energy that has to be supplied to the collision system, in the laboratory frame, is equal to 16.5 MeV/u. The reaction energies for all the RTE and RT2E transitions investigated in this work are shown in Table 1 along with the corresponding binding energies of the initial and intermediate states of the projectile ions Kr^{34+} and O^{q+} (q=5,6).

The third mechanism investigated here, namely, radiative electron capture (REC), is a process which occurs in an ion-atom collision when electron capture is accompanied by simultaneous x-ray emission. REC involving capture to the M-shell, i.e., REC-M, is illustrated schematically for a heliumlike projectile ion in Figure 9.

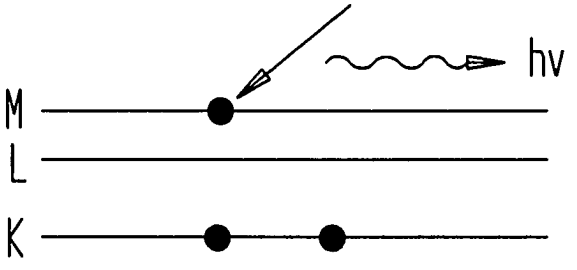

Figure 9. Schematic of REC Associated With Electron Capture Into the M-shell of the Projectile Ion.

Table 1

Reaction Energies for RTE and RT2E Transitions Investigated in This Work Along With the Corresponding Binding Energies of the Initial and Intermediate States of the Projectile Ions Kr^{34+} and O^{q+} (q=5,6)

Ion	State	Binding Energy (keV)
Kr^{34+}	$1s^2$	-35.230
Kr^{33+}	$2s^22p$	-13.000
	1s2s2p	-26.400
O^{6+}	$1s^2$	-1.606
O^{5+}	$2s^22p$	-0.560
	1s2s2p	-1.191

Krypton: RT2E reaction energy: $1s^2 \rightarrow 2s^22p$: → 40.5 MeV/u

RTE reaction energy: $1s^2 \rightarrow$ 1s2s2p: → 16.5 MeV/u

Oxygen : RT2E reaction energy: $1s^2 \rightarrow 2s^22p$: → 1.91 MeV/u

RTE reaction energy: $1s^2 \rightarrow$ 1s2s2p: → 0.75 MeV/u

REC is completely analogous to radiative recombination (RR) involving a similar interaction with a free electron. RR is simply the inverse of the photoelectric effect and, hence, has been treated[26] theoretically as such. The total radiative recombination cross section for bare ions colliding with free electrons is given by[26]

$$\sigma_{rec}=9.1\left(\frac{\eta^3}{1+\eta^2}\right)^2 \frac{e^{-4\eta\arctan(\frac{1}{\eta})}}{1-e^{-2\pi\eta}} 10^{-21} cm^2 \qquad (2.9)$$

Here $\eta=Ze^2/\hbar v$ is the Sommerfeld parameter (or Coulomb

parameter), Z is the atomic number of the ion, e is the electron charge, and v is the original relative velocity between electron and nucleus. However, photons emitted in the RR (and REC) process have a $\sin^2\theta$ dependence, and so the differential cross section is given by[26]:

$$\frac{d\sigma_{rec}}{d\Omega}=\sigma_{rec}\frac{3}{8\pi}\sin^2\theta \qquad (2.9')$$

The angle θ denotes the angle between v and the direction of the emitted photon.

In an ion-atom collision, however, the electrons to be captured are not free but are bound to the target nucleus, and therefore have a momentum distribution. If the velocity of the ion is considerably greater than the orbital velocity of the target electron to be captured, then, based upon the impulse approximation, the cross section can be written[27] as:

$$\frac{d^2\sigma}{d\Omega d\hbar\omega}=\int d^3p\frac{d\sigma_{rec}}{d\Omega}|\psi_i(p-p_0)|^2\,\delta(E_f-E_i) \qquad (2.10)$$

The δ-function guarantees energy conservation and $|\Psi_i(p-p_0)|^2$ is the initial electronic momentum distribution, which is peaked around $p_0 = mv$ because the electron is moving with this average momentum towards the projectile which is considered to be at rest. In the impulse approxi-

mation the initial electronic potential V_i remains constant[27] during the capture process and so:

$$E_i=\frac{(p_0+p_i)^2}{2m}+V_i=-\epsilon_i+\frac{p_0^2}{2m}+\boldsymbol{v}\cdot\boldsymbol{p}_i \qquad (2.11)$$

where ϵ_i is the initial electronic binding energy. Furthermore,

$$E_f=-\epsilon_f+\hbar\omega \qquad (2.12)$$

where ϵ_f is the final electronic binding energy and $\hbar\omega$ is the energy of the emitted x ray. By combining equations 2.11 and 2.12 it is seen that the energy of the emitted photon depends on the electronic momentum component, p_{iz}, parallel to v:

$$\hbar\omega=\epsilon_f-\epsilon_i+\frac{p_0^2}{2m}+vp_{iz} \qquad (2.13)$$

If the projectile ion is much heavier than the target then the REC cross section is peaked around $p_i = 0$ and Eq. (2.13) becomes :

$$\hbar\omega=\epsilon_f+\epsilon_i+\frac{p_0^2}{2m} \qquad (2.14)$$

For a light target ϵ_i is negligibly small. Therefore the energy centroid of the emitted x rays is given by:

$$E_{REC}=\epsilon_f+\frac{m_e}{M}E \qquad (2.15)$$

where all quantities are measured in the projectile ion frame. Each (centroid) REC x-ray energy (relativistic[25]) associated with capture into L, M,.. shells of the projectile Kr^{34+} ions, for the projectile energies investigated in this work, are listed in Table 2.

Table 2

Rec X-Ray Energies (Centroids) Associated With Capture Into L, M, ... Shells of the Projectile Kr^{34+} Ions for the Projectile Energies Investigated in This Work

Beam Energy (MeV/u)	X-ray energy (keV)		
	REC-L	REC-M	REC-∞
37.2	24.5	22.2	20.4
39.2	25.6	23.3	21.5
40.2	21.2	23.8	22.1
41.2	26.7	24.4	22.6
43.2	27.8	25.5	23.7
47.5	30.2	27.8	26.1

CHAPTER III

EXPERIMENTAL PROCEDURE

Kr^{34+} + H_2 Measurements

The Kr^{34+} + H_2 measurements were made at the National Superconducting Cyclotron Laboratory (NSCL) at Michigan State University. The choice of H_2 as a target was dictated by the desire to keep the "background" from nonresonant processes[2,3] small and to use a target with only two electrons as has been the case for most studies of RTE. The desired beam energy was obtained and the charge state selected using the energy degrader and the A1200 beam analysis device at NSCL.[28] A schematic of the experimental apparatus is shown in Figure 10. The arrangement and techniques are very similar to those used previously[4] for the investigation of RTE.

A projectile beam composed of Kr^{34+} ions was accelerated and directed into a differentially pumped gas cell containing the H_2 target molecules. Two sets of slits were used to collimate the incident beam. As the projectile goes through the target cell, it can interact with a target molecule and form the intermediate state characteristic of RTE or RT2E (or NTE). The excited state can then decay by

emitting x rays. Since the formation of the intermediate state requires the capture of a target electron by the ion, the projectile ion becomes less positive (i.e., q → q-1, where q is the projectile charge), and can be detected by

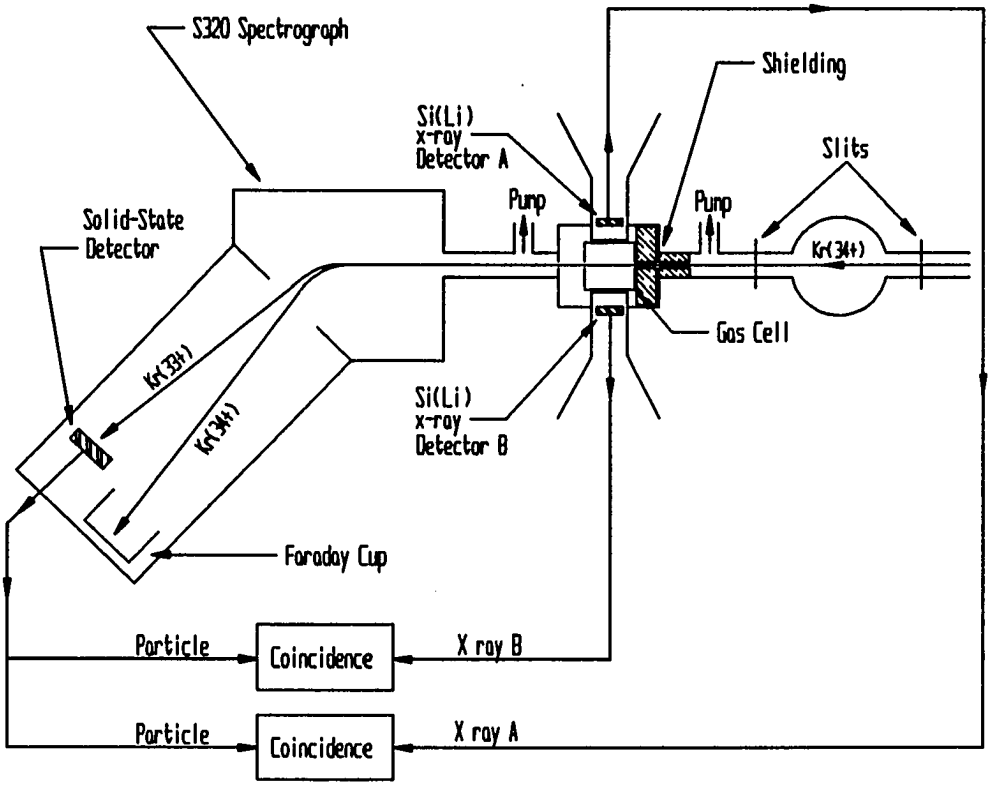

Figure 10. Schematic of the Experimental Apparatus.

magnetic separation of the charge-changed components of the projectile beam emerging from the gas cell. By collecting the charge-changed components and the non-charge-changed component, the fraction of projectile ions that have undergone capture can be determined. However, in order to

determine that an intermediate excited state characteristic of RTE or RT2E has been formed, an x ray which results from the relaxation of the excited state (see Chapter II) must also be detected. In this work, detection of a K x ray implies that excitation of the projectile K-shell took place in the collision interaction. Since a heliumlike ion has two electrons initially in the K-shell (the lifetime[29] of metastable states in Kr^{34+} is about 1 ns), the only way K x-ray emission can occur is for at least one of the two K-shell electrons to be promoted to a higher shell.

For the x-ray detection, two Si(Li) detectors, labeled A and B, were mounted at 90^0 to the beam axis as shown in Figure 10. This arrangement of two detectors provided a larger solid angle which improved the quality of the experimental statistics. In addition, the use of two detectors allowed for the detection of coincidences between photons emitted 180^0 apart during the decay of the excited ions (see Chapter IV).

The beam components emerging from the collision region were separated by the S320 spectrograph which was used as a charge-state analyzing device following the target region. Finally, a solid-state detector was used to detect the charge-changed (single capture) beam component while a Faraday cup was used to collect the main beam component.

A schematic of the electronics is shown in Figure 11. Signals from each Si(Li) detector were routed through a

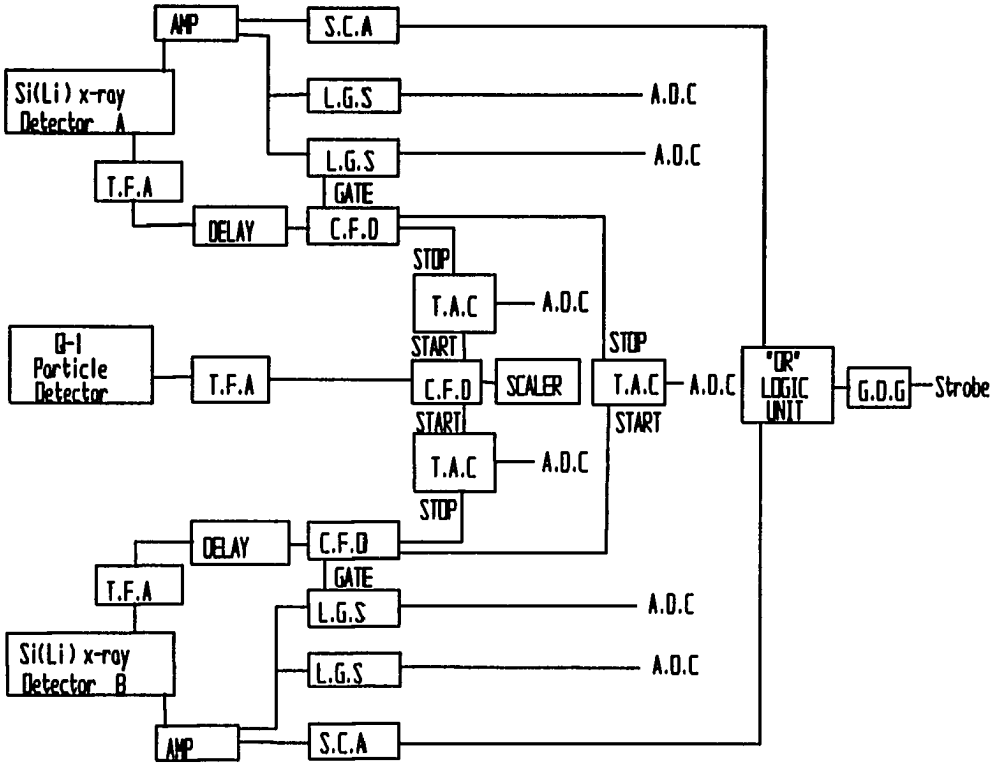

Figure 11. Schematic of Electronics for Signal Processing.

Key to Abbreviations

T.F.A	=	**Timing Filter Amplifier**
C.F.D.	=	**Constant Fraction Discriminator**
S.C.A	=	**Single Channel Analyzer**
G.D.G	=	**Gate and Delay Generator**
L.G.S	=	**Linear Gate Stretcher**
T.A.C	=	**Time-to-Amplitude Converter**
A.D.C	=	**Analog/Digital Converter**

timing filter amplifier (TFA) and a constant fraction discriminator (CFD), which outputs a logic signal when the amplitude of the analog x-ray pulse exceeds the discriminator level setting. The logic signal from the CFD provided the STOP signal for a time-to-amplitude converter (TAC) and

a similar set of electronics from the particle detector provided the START signal. This particular arrangement was dictated by the desire to keep the accidental coincidence events as small as possible (i.e., the capture event rate was very small relative to the x-ray emission rate). The TAC gives an analog output pulse whose amplitude is proportional to the time difference between the START and STOP signals. Thus, a TAC output occurred any time an x-ray event and a capture event were detected within a preset time period (2 μsec in this case). In this way a time spectrum is constructed for each run (i.e., coincidence counts versus time). In addition, the total x-ray emission (number of x-ray events versus x-ray energy) was recorded as was the total number of capture events.

Typical time spectra corresponding to x-ray emission coincident with capture are shown for both detectors in Figure 12. All of the data were collected in "event mode" and saved on magnetic tape by using the NSCL data acquisition program SARA.

The data analysis was done at WMU using the data acquisition and analysis program CHAOS. A FORTRAN program was written in order to convert the original format of the data files into one suitable for use with CHAOS. Coincidence x-ray spectra were generated from software sorting routines in the data acquisition program. These sorting routines are used to associate x-ray events with coinci-

dence events from the TAC, thereby producing an x-ray coincidence spectrum. Typical energy spectra of x rays coincident with capture are shown for both detectors in Figure 13.

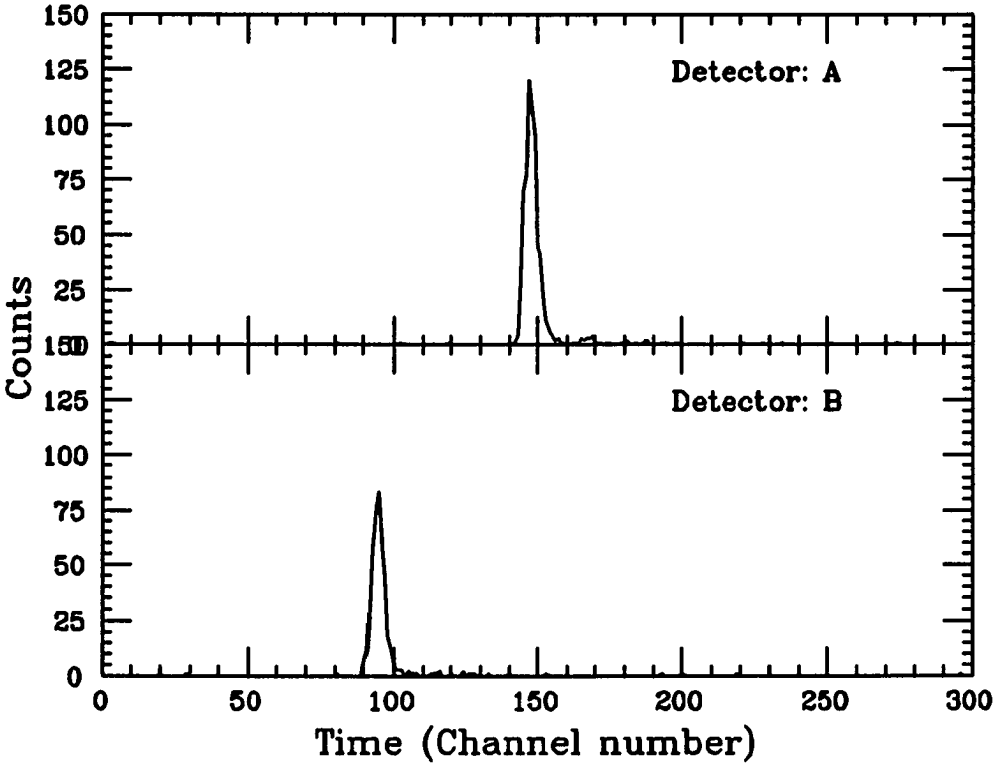

Figure 12. Typical TAC Spectra for X Rays Coincident With Capture for 16.5 MeV/u Kr^{34+} + H_2 Collisions at 50 mTorr Gas Cell Pressure.

Data were taken for two projectile energy regions: 15.5-17.5 MeV/u (the RTE maximum occurs near 16.5 MeV/u) and 37.2-47.5 MeV/u (the RT2E maximum is expected to occur near 40.5 MeV/u). RTE was measured first to test the experimental setup, and to provide a benchmark for the RT2E measurements. Data were collected for several target gas

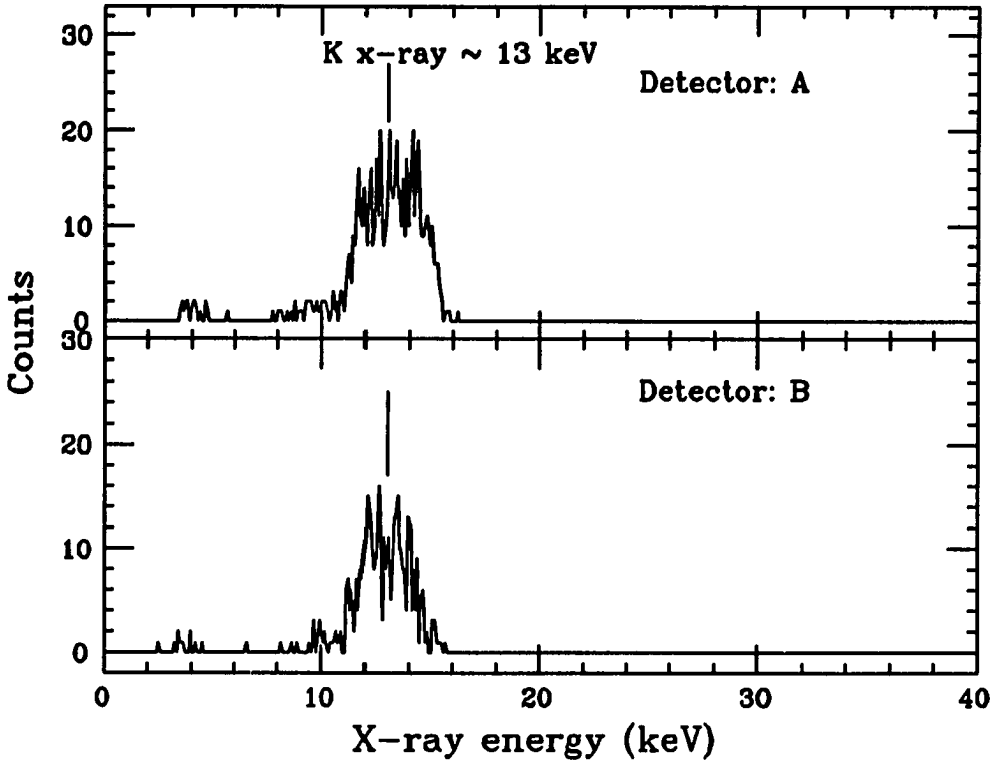

Figure 13. Spectra for X Rays Coincident With Capture for 16.5 MeV/u Kr^{34+} + H_2 Collisions at 50 mTorr Gas Cell Pressure.

cell pressures at each projectile energy in order to verify the linear dependence of the charge-changed and x-ray event fractions with respect to the gas cell pressure. This is necessary since linearity ensures that single-collision conditions prevail. At least three runs for each projectile energy (typically 0, 50, and 80 mTorr) were conducted in the energy range of 15.5-17.5 MeV/u. The total coincidence counts were obtained by integrating the region of interest (the peak region in Figure 13) of each spectrum. By plotting the yield (i.e., number of counts divided by the

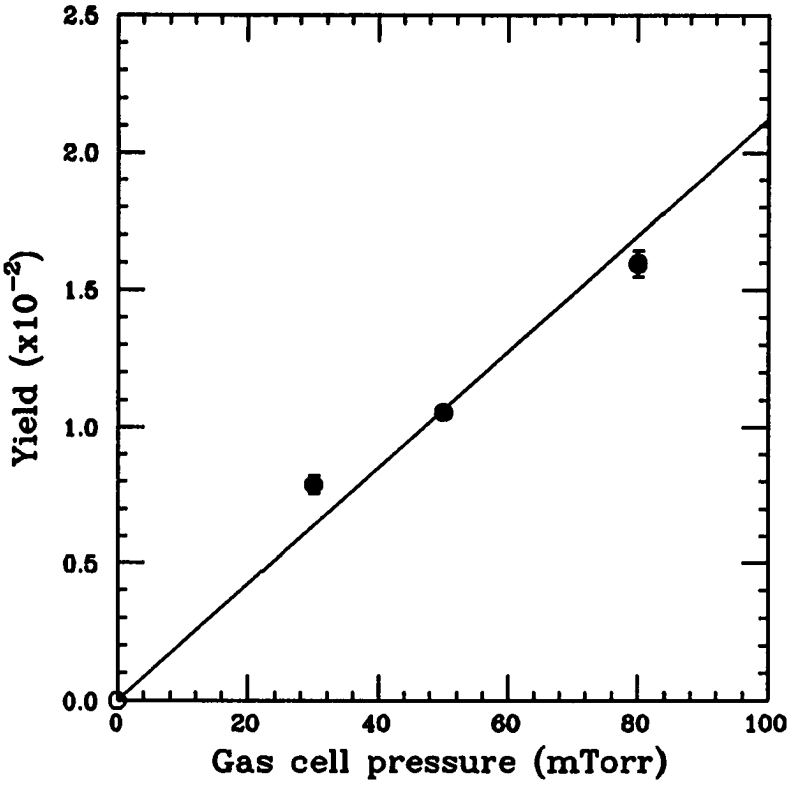

Figure 14. Plot of Coincidence Yield Versus the Gas Cell Pressure for 16.5 MeV/u Kr^{34+} + H_2.

number of incident ions) of coincidence counts versus the gas cell pressure, one can verify the linear dependence of the measured yields with respect to the gas cell pressure (see Figure 14). For the 37.2-47.5 MeV/u energy region, however, total x-ray and coincidence yields were measured only at 80 and 0 mTorr target gas pressures because of very low counting rates.

O^{q+}(q=5,6) + He Measurements

The O^{q+}(q=5,6) + He measurements were made at Western

Michigan University using the EN tandem Van de Graaff accelerator. A general schematic of the accelerator is shown in Figure 15. Negative oxygen ions (q=-1) extracted from the "exchange ion source" were accelerated towards the positive terminal of the accelerator, where they were directed through a stripping gas cell. As the ions go through the gas a number of electrons are stripped off and the ions become positive. The ions are then repelled by the positive terminal voltage, and accelerated a second time thereby gaining a total kinetic energy V(q+1), where V is the positive voltage on the terminal and q (q=1,2..) is the charge state of the positive ions emerging from the stripper gas. O^{q+}(q=5,6) ions were selected by an analyzing magnet and then directed into the atomic physics beam line (see Figure 16).

The interactions taking place inside the target gas cell are identical to the ones described previously for the Kr^{34+} + H_2 system. For the O^{6+} + He collision system, however, detection of a K x ray does not necessarily imply that excitation of the projectile K-shell took place in the collision interaction. This is due to the fact that the lifetime[29] of O^{6+} (1s2s) metastable states is sufficiently long (~1 ms) so that a fraction of the projectile ions have electron configurations other than $1s^2$ when they reach the target. In this case, electron capture into shells with n > 1 can result in K x-ray emission during the n=2 → 1

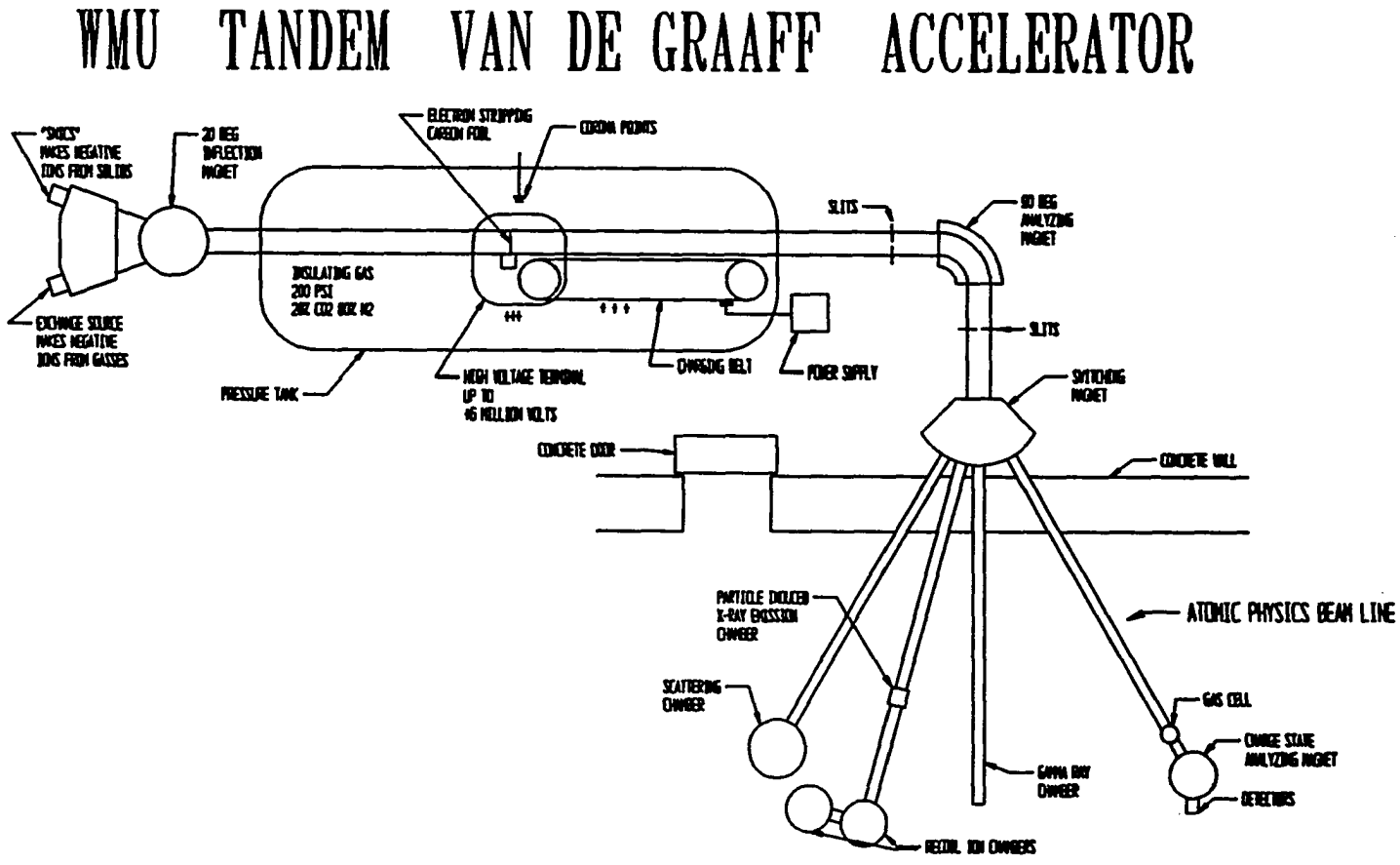

Figure 15. Schematic of the WMU Accelerator.

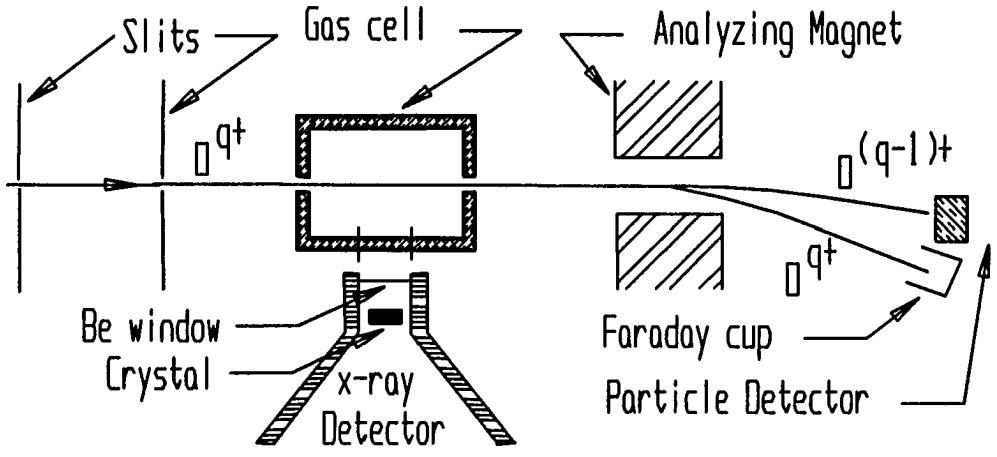

Figure 16. **Schematic of the Atomic Physics Beam Line at WMU.**

decay of the captured electron.

For the x-ray detection, a single Si(Li) detector, with a 7.62 μm Be window to detect low energy x rays, was mounted at 90^0 to the beam axis as shown in Figure 16. Two sets of slits were used to collimate the incident beam. The beam components were separated by a magnet following the target gas cell. The charge-changed (single capture) beam component and the main beam were detected by a solid-state detector and a Faraday cup, respectively.

A schematic of the electronics used for the O^{q+} + He measurements is shown in Figure 17. The electronics setup is similar to the one used for the Kr^{34+} + H_2 measurements. For this collision system, however, the signals from the Si(Li) detector were routed through a spectroscopy amplifier (instead of a timing filter amplifier) which was used as

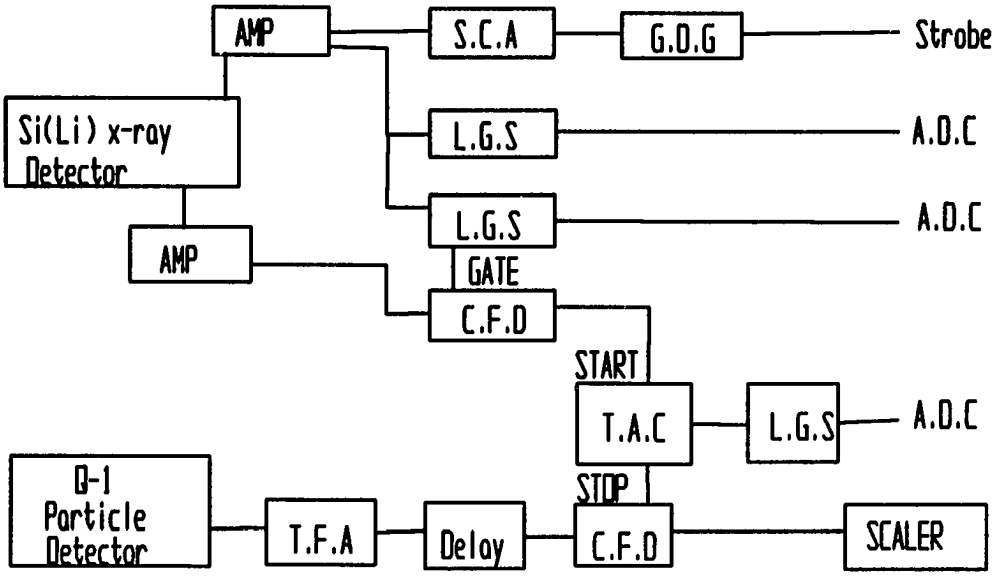

Figure 17. Schematic of the Electronics for Signal Processing for the O^{q+} + He Measurements.

For Key to Abbreviations see Figure 11.

a "timing" amplifier. This was dictated by the fact that the K x rays for oxygen (about 630 eV) gave a very small amplitude electronic pulse only slightly bigger than the electronic noise. Also, since the x-ray emission rate was significantly lower than the single-capture particle rate, the logic signal from the x-ray CFD provided the START signal for the time-to-amplitude converter (TAC) and a similar set of electronics for the particle detector provided the STOP signal. This arrangement served to reduce the accidental coincidence events significally. Coincidence time spectra, total x-ray emission spectra, and the total number of capture events were recorded. A typical time

(TAC) spectrum corresponding to K x-ray emission coincident with capture is shown in Figure 18.

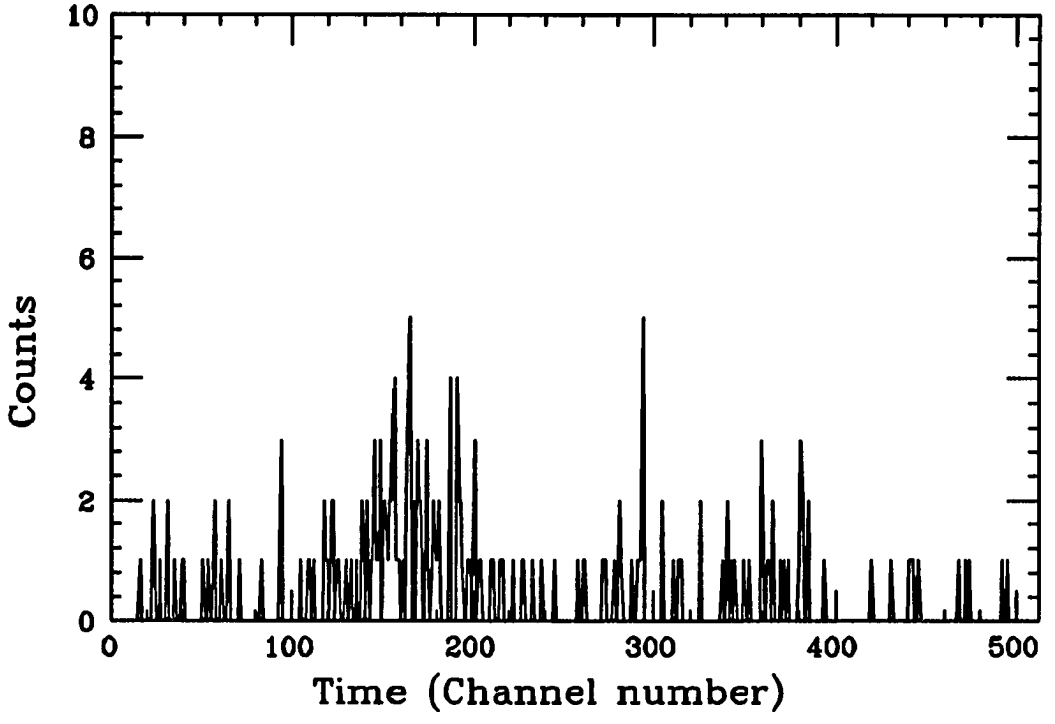

Figure 18. TAC Spectrum for 12 MeV O^{6+} + He Collisions at 80 mTorr Gas Cell Pressure.

All of the data were collected in "event mode" and sorted using a MicroVAX II computer system which was interfaced to the signal processing electronics. As in the case of the Kr^{34+} + H_2 data, the analysis was done by using the data acquisition and analysis program CHAOS. A typical spectrum of x rays coincident with capture is shown in Figure 19. For the O^{6+} + He collision system, data were taken for the projectile energy region: 11-33 MeV (The RTE maximum[21] occurs near 13 MeV, while the RT2E maximum is expected to

occur near 30.5 MeV). In addition, data were taken for the O^{5+} + He collision system at two projectile beam energies: 12.8 and 30.5 MeV. In the next chapter the results of all the experimental work are presented.

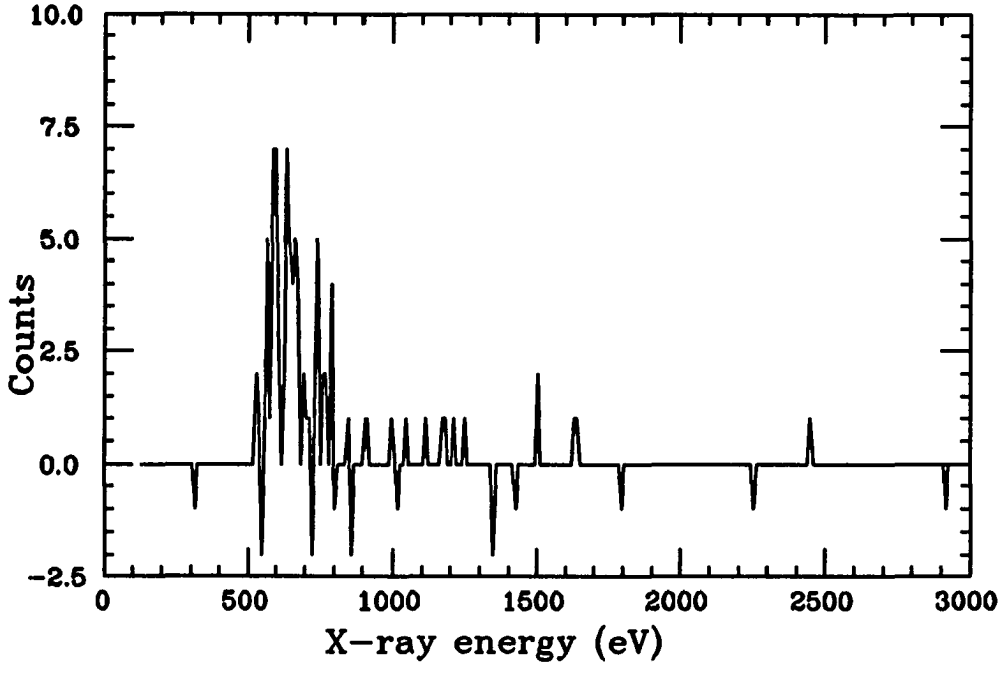

Figure 19. Spectrum of X Rays Coincident With Capture for 12 MeV O^{6+} + He Collisions at 80 mTorr Gas Cell Pressure (Background Has Been Subtracted Thereby Accounting for the Negative Counts).

CHAPTER IV

DATA ANALYSIS AND RESULTS

Determination of Cross Sections

The number of x-ray events (total or coincidence) which are detected (see CHAPTER III) depends on the integrated incident beam intensity, the thickness of the target, the geometry of the gas cell, the cross section, the efficiency of the x-ray detectors, and the solid angle subtended by the detectors. Mathematically, the number of observed events is given by:

$$I = I_0 T \sigma \epsilon \left[\frac{\Delta\Omega}{4\pi}\right] \qquad (4.1)$$

$$= I_0 (N_0 PL)\, \sigma \epsilon \left[\frac{\Delta\Omega}{4\pi}\right] \qquad (4.2)$$

where

- I is the number of x-ray events detected (see Figures. 10 and 16),
- I_0 is the total number of incident ions that pass through the target cell,
- σ is the cross section of interest,
- ϵ is the detector efficiency,

$\Delta\Omega$ is the solid angle subtended by the detector,

T is the target thickness in (atoms/cm^2) and is equal to the quantity N_0PL, where

N_0 is a constant (3.3 X 10^{13} atoms/cm^3.mTorr),

P is the gas cell pressure in mTorr,

L is the effective length of the gas cell in cm,

In the case of the Kr^{34+} measurements, Eq. (4.1) holds separately for each of the detectors A and B (see Figure 10).

Then, defining $F=I/I_0$ Equation 4.2 gives:

$$F=\frac{I}{I_0}=\sigma N_0 LP\left[\frac{\Delta\Omega}{4\pi}\right]\epsilon \qquad (4.3)$$

where F is the fraction of the x-ray events that are detected. Since σ is a constant for a particular beam energy, Equation 4.3 indicates that F depends linearly on P. For each incident projectile energy, measurements were taken for several different target pressures (each measurement at a well-defined gas cell pressure) to establish this linear dependence of F versus P. (see Figure 14). From Equation 4.3,

$$\sigma=\left(\frac{\Delta F}{\Delta P}\right)\left[N_0 L\frac{\Delta\Omega}{4\pi}\epsilon\right]^{-1}=C\left(\frac{\Delta F}{\Delta P}\right) \qquad (4.4)$$

where $C=[N_0L(\Delta\Omega/4\pi)\epsilon]^{-1}$, and so the cross section of interest is proportional to the slope of the F vs. P curve. Equation 4.4 is then used to calculate the total absolute cross sections. Similar expressions may be derived for

differential cross sections $d\sigma/d\Omega$. For this latter case Equations 4.3 and 4.4 become:

$$F=\frac{I}{I_0}=\frac{d\sigma}{d\Omega}N_0LP\Delta\Omega\epsilon \qquad (4.5)$$

and

$$\frac{d\sigma}{d\Omega}=\left(\frac{\Delta F}{\Delta P}\right)[N_0L\Delta\Omega\epsilon]^{-1}=C'\left(\frac{\Delta F}{\Delta P}\right) \qquad (4.6)$$

where $C'=[N_0L\Delta\Omega\epsilon]^{-1}$.

Since REC cross sections depend on a $\sin^2(\theta)$ factor[27] (θ is the angle between the direction of the incident beam and the direction of the emitted x ray) there is an anisotropy which depends on the viewing angle (90 degrees in this case). The measured differential REC cross sections (at 90^0) were obtained from Equation 4.6. The total REC cross section is given by:

$$\sigma=\frac{3}{8\pi}\frac{d\sigma}{d\Omega}(90^0) \qquad (4.7)$$

For the RTE mechanism, however, the anisotropy is relatively small[30] (< 20%) and so Equation 4.4 was used to calculate the experimental total RTE cross sections.

Kr^{34+} + H_2 Measurements

As discussed earlier, Figure 13 shows typical spectra of x rays coincident with single electron capture for the two detectors, A and B, for 16.5 MeV/u Kr^{34+} + H_2, which is

near the energy where RTE involving KLL transitions (i.e., excitation to the L shell is accompanied by capture to the L shell) maximum should occur. In these spectra, Kr K x rays of energy ~ 13 keV are clearly seen. To obtain the cross sections, the total events seen by both detectors were summed.

However, to determine the absolute cross sections it was necessary to determine the intrinsic relative efficiency of the two detectors. From Eq. (4.1) we note that

$$\frac{I_A}{I_B}=\frac{\epsilon_A \Delta\Omega_A}{\epsilon_B \Delta\Omega_B}=\epsilon_r' \qquad (4.8)$$

The ratio I_A/I_B was measured using radioactive sources for several source-detector distances. A Co^{57} γ-ray source was used for 14 keV photons, while a Cd^{109} x-ray source was used for 22 keV x-rays. Figure 20 shows the measured relative number of counts (I_A/I_B) as a function of the detector-source distance. For a beam-detector distance of 1 cm (actual beam-detector distance for the Kr measurements), ϵ_r' is equal to an average of about 1.4. Figure 21 shows the measured number of counts for the Kr^{34+} + H_2 measurements for detector A divided by the "corrected" number of counts for detector B (i.e., multiplied by the intrinsic relative efficiency) for each of the projectile beam energies investigated. It is seen that I_A/I_B is nearly unity for the data obtained in this work. This result implies

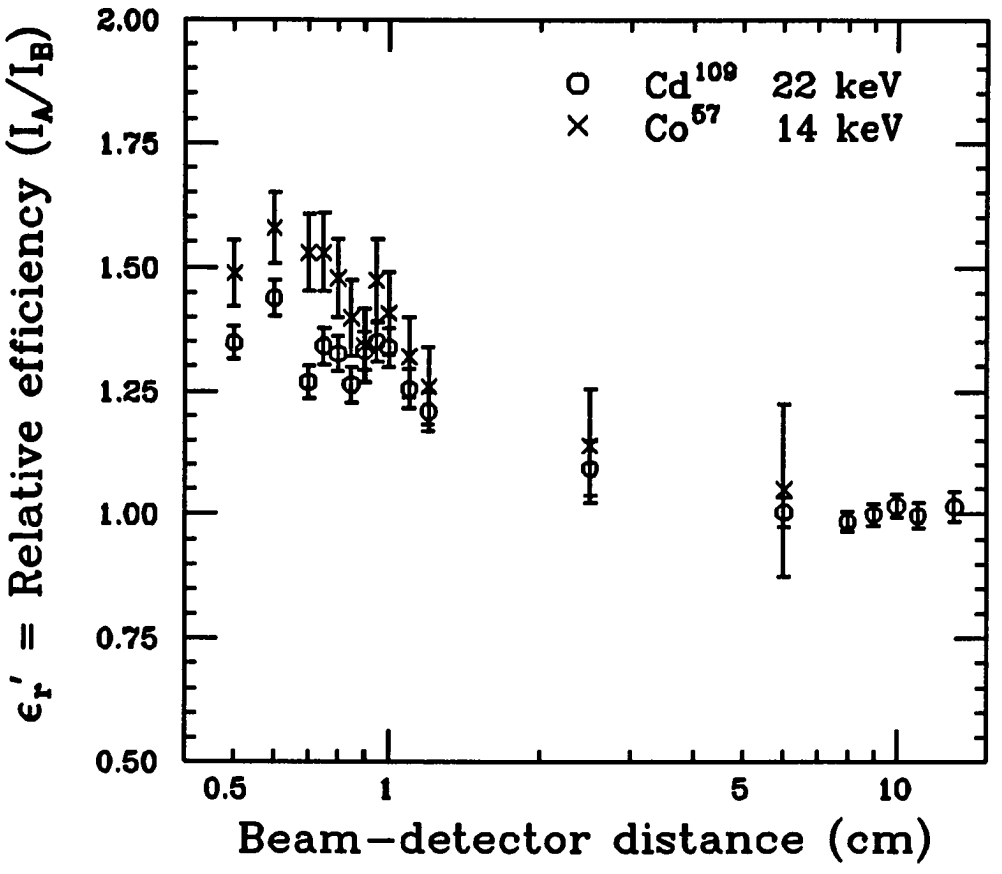

Figure 20. Intrinsic Relative Efficiency as a Function of the Beam-Detector Distance for Detectors A and B as Measured With a Co^{57} Source and a Cd^{109} Source.

that no factor other than the intrinsic relative efficiencyis responsible for the difference between the number of events recorded by the two detectors.

The cross sections derived from these spectra, along with theoretical calculations[9] of RTE, are shown in Figure 22, where a pronounced maximum is observed to occur near 16.5 MeV/u beam energy as expected. It is seen that the

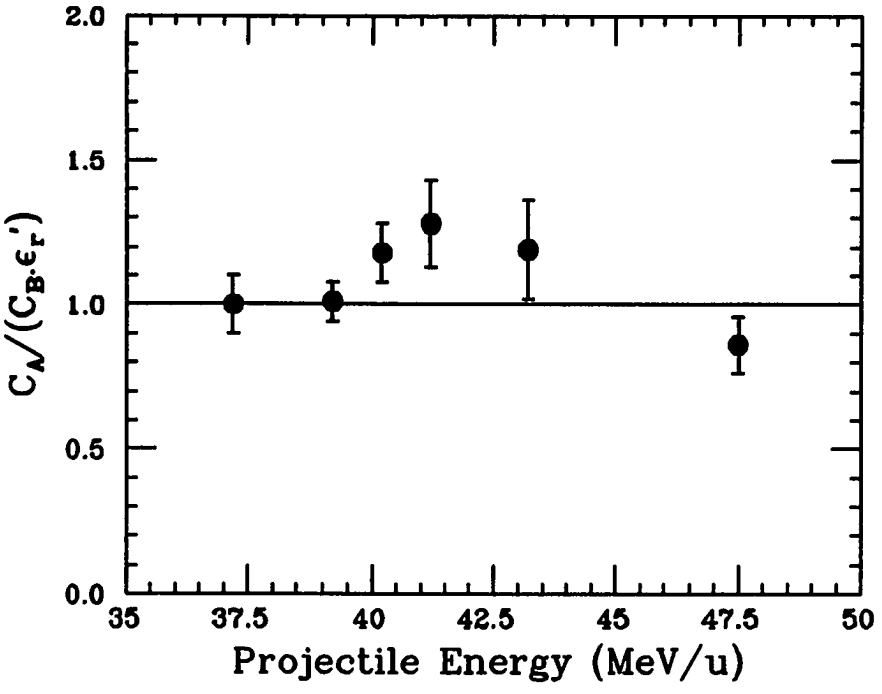

Figure 21. Number of Counts for the Kr^{34+} + H_2 Measurements for Detector A Dividedby the "Corrected" Number of Counts for Detector B (i.e., Multiplied by the Intrinsic Relative Efficiency from Figure 20).

measured cross sections are systematically larger than the theoretical values but the discrepancy is within the systematic error of about 30%. Related measurements of RTE for Kr^{35+} ions have previously been reported by Stöhlker.[31]

Spectra for x rays coincident with capture in the projectile energy region 37.2-47.5 MeV/u (the RT2E maximum involving KKLLL transitions is expected to occur near 40.5 MeV/u) are shown in Figures 23 and 24 for detectors A and B respectively. (The notation KKLLL means double excitation to the L-shell is accompanied by capture to the L-shell).

All of the spectra were normalized to the one associated with the 37.2 MeV/u beam energy so that the relative number of coincidence events can be compared for each spectrum. It

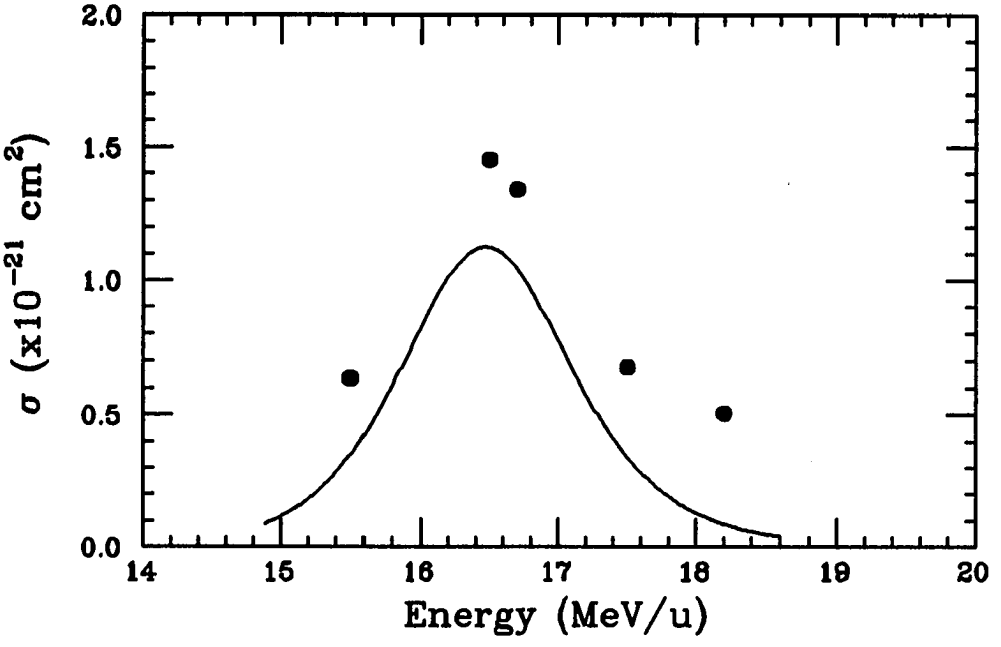

Figure 22. RTE Cross Sections for Kr^{34+} + H_2.

The solid curve is the calculated RTE cross section. The statistical errors are about the size of the symbols; the overall systematic uncertainty is estimated to be less than about 30%.

is seen that there are essentially no real coincidences associated with Kr K x rays (near 13 keV), in contrast to the RTE results shown in Figure 13. One explanation for this observation would be that the triply-excited intermediate states formed in RT2E decay principally by first emitting an x ray and then by ejecting an Auger electron (or vice versa), thus returning the projectile ion to its

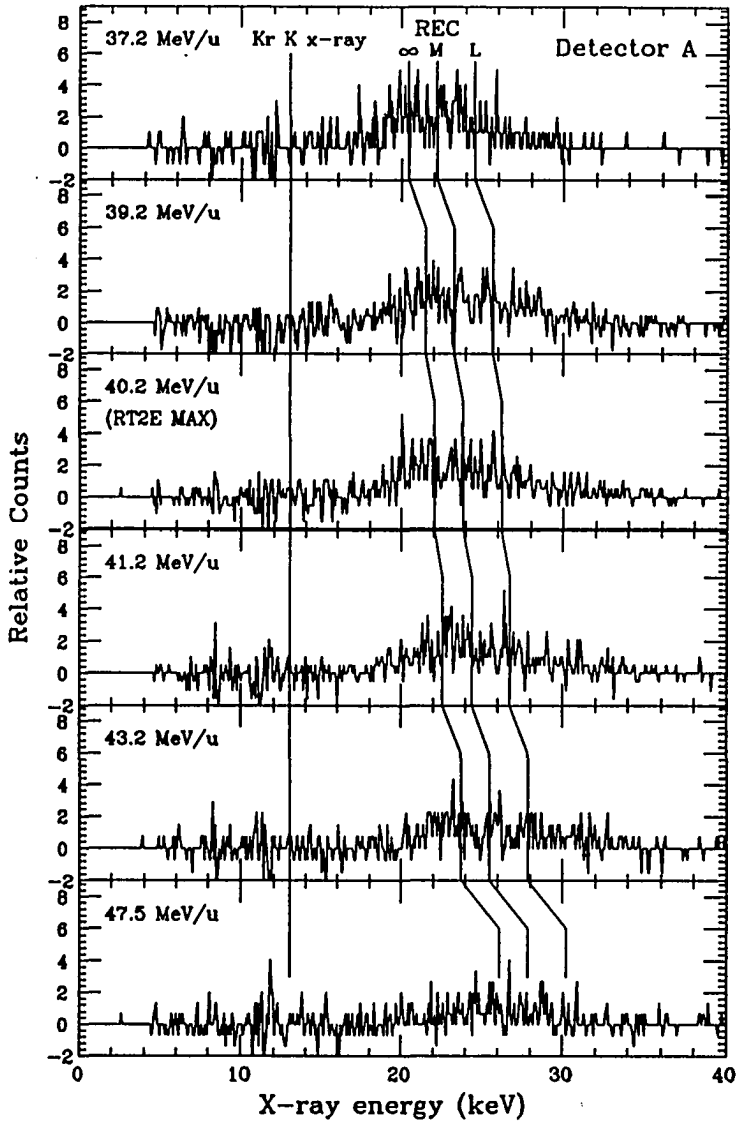

Figure 23. Spectra of X Rays Coincident With Single-Electron Capture for Detector A (see Figure 10) in the Projectile Energy Region 37.2-47.5 MeV/u.

The expected position of Kr K x rays is indicated as well as the expected centroid energies for REC to the L shell, M shell, and series limit (∞) respectively, (see text).

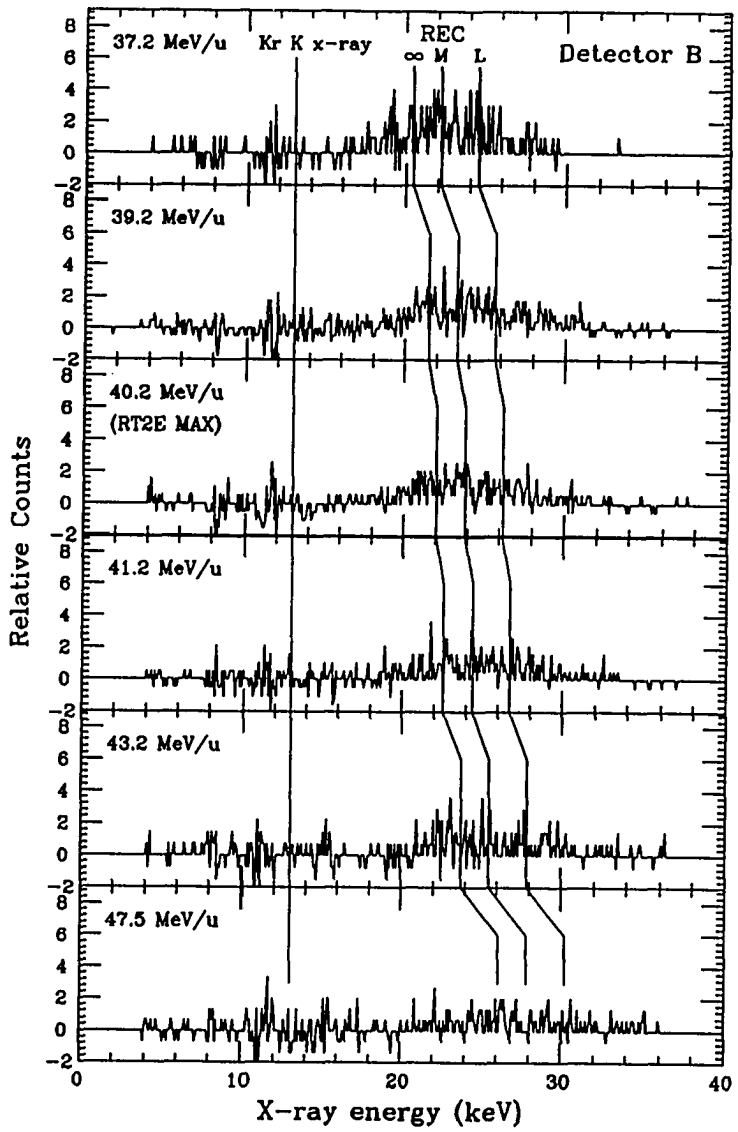

Figure 24. Spectra of X Rays Coincident With Single-Electron Capture for Detector B (see Figure 10) in the Projectile Energy Region 37.2-47.5 MeV/u.

The expected position of Kr K x rays is indicated as well as the expected centroid energies for REC to the L shell, M shell, and series limit (∞) respectively, (see text).

original charge state. In this case, RT2E events would not be observed by detecting x-ray events coincident with electron capture. As discussed above, (see Chapter II) a theoretical estimate[9] of the RT2E cross section for KKLLL transitions involving radiative stabilization by two sequential photons gives about 10^{-27} cm^2, while the RT2E cross section for one photon followed by Auger emission (or vice versa) is about 10^{-28} cm^2. The sensitivity of the present measurements is about 10^{-25} cm^2. So, for this sensitivity it would not be possible to observe RT2E unless the theoretical results are a severe underestimate.

Coincidences do exist, however, for higher x-ray energies (> 20 keV), as seen in Figures 23 and 24. (The electronic setup permitted the observation of coincidence events for x-ray energies as high as 40 keV.) From the figure it is seen that there is an apparent shift, with beam energy, in the centroid energy of these high-energy x-ray events, a feature which is characteristic of the radiative electron capture (REC) mechanism (see Eq. 2.15). The positions labeled REC-L, REC-M, and REC-∞ are the expected centroid x-ray energies for REC associated with electron capture into the L, M, and n=∞ (zero binding energy) shells, respectively.

The measured differential cross sections, observed at 90^0 with respect to the beam axis, associated with electron capture coincidences for x-ray energies > 20 keV are shown

in Figure 25 along with the calculated values[30] for REC. There is reasonable overall agreement between experiment and theory, and the measured cross sections decrease monotonically with beam energy as does the REC theoretical

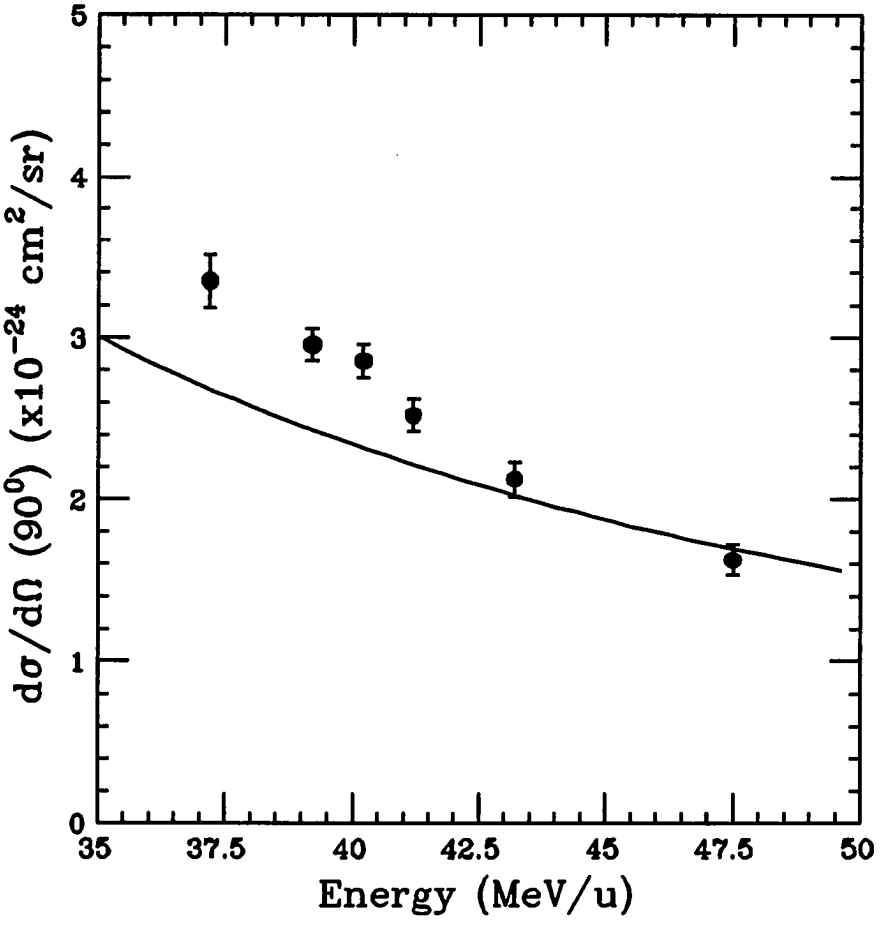

Figure 25. Measured Differential Cross Sections at 90^0 for X Rays Coincident With Capture for X-Ray Energies >20 keV.

Error bars are relative uncertainties based on the total number of observed events for both detectors. The overall systematic uncertainty is estimated to be about 30%. The solid curve is the calculated REC cross section.

prediction. However, there seems to be a systematic discrepancy at the lower beam energies investigated. The reason for this discrepancy is unknown.

Finally, Figure 26 shows a time spectrum (TAC) for coincidences between photons emitted 180^0 apart for 40.2 MeV/u Kr^{34+} + H_2 collisions at 80 mTorr gas cell pressure. Figure 27 shows the corresponding x-ray energy spectrum for these 180^0 photons associated with single electron capture events. The results indicate that there are essentially no real coincidences associated with these events.

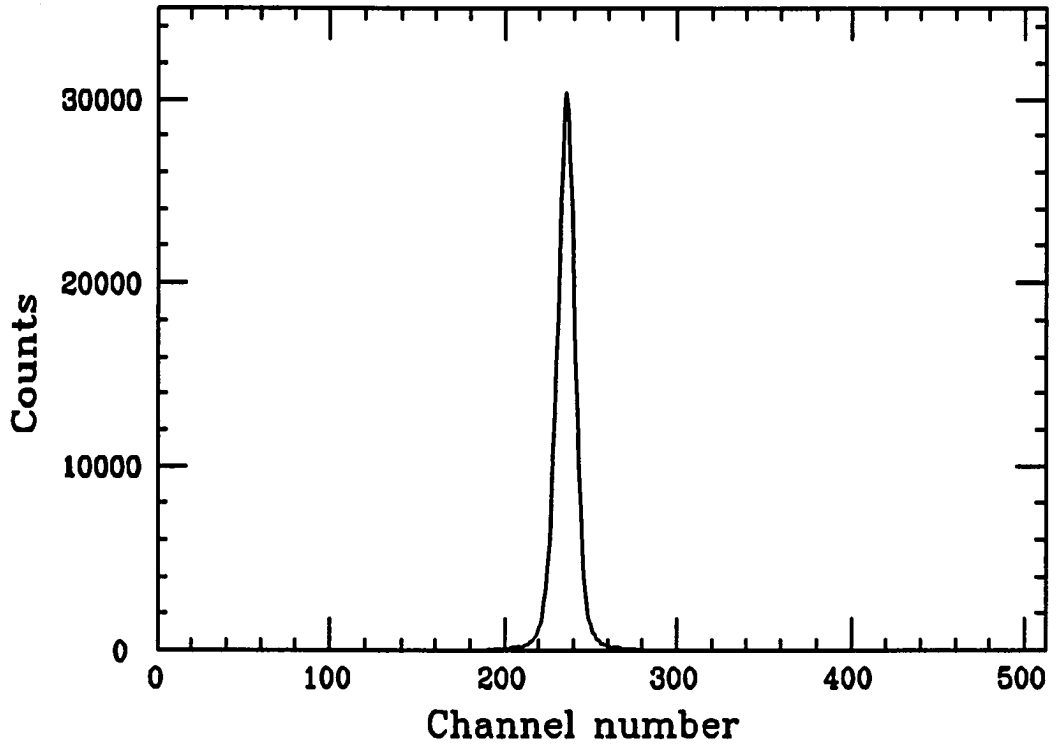

Figure 26. TAC Spectrum for Photons Emitted 180^0 Apart for 40.2 MeV/u Kr^{34+} + H_2 Collisions at 80 mTorr Gas Cell Pressure.

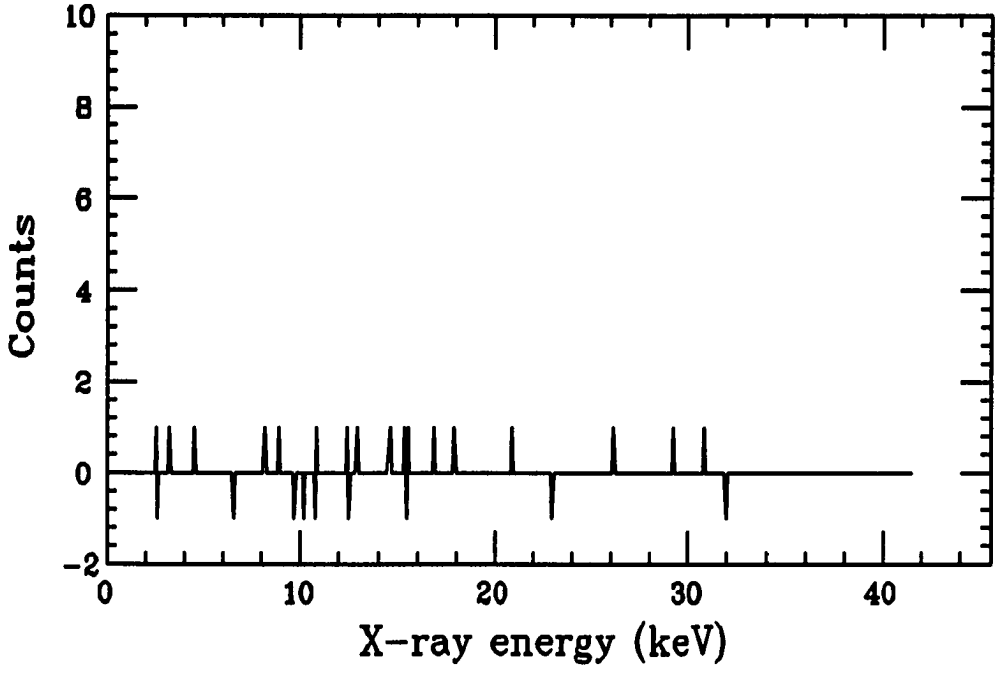

Figure 27. X-ray Energy Spectrum for Coincidences Between Photons Emitted 180^0 Apart and Associated With Capture Events for the Collision System Mentioned Above.

$O^{5,6+}$ + He Measurements

The choice of O^{q+} as a projectile was dictated by the desire to investigate RT2E for relatively low Z ions. The data analysis for these measurements is similar to the analysis associated with the Kr^{34+} + H_2 data discussed above.

Figure 28a shows a time spectrum for x rays coincident with capture (TAC) for 12.8 MeV O^{5+} + He collisions (near the expected KLL RTE maximum) at 25 mTorr gas cell pressure. It is seen that essentially no real coincidences are

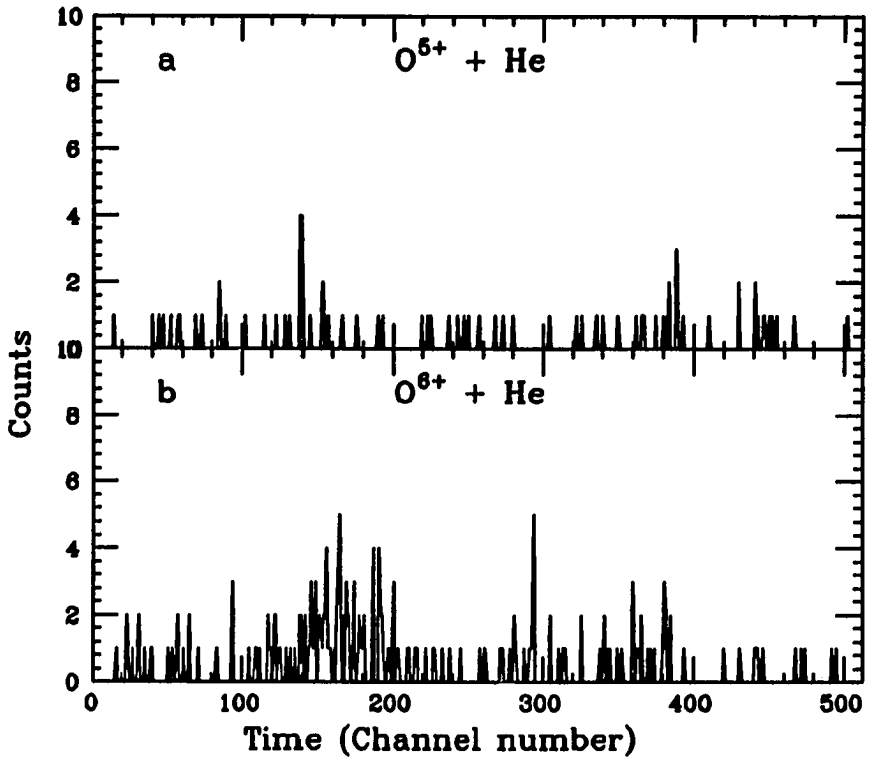

Figure 28. a) TAC Spectrum for 12.8 MeV O^{5+} + He Collisions at 80 mTorr Gas Cell Pressure; b) TAC Spectrum for 12 MeV O^{6+} + He Collisions at 80 mTorr Gas Cell Pressure.

associated with this particular collision system within the sensitivity of the measurements. This is in part due to the fact that the intermediate doubly excited state of a four-electron ion with small Z (Z=8 in this case) is more likely to decay by electron (Auger) emission rather than by x-ray emission.[21] In addition, x rays that may result from the relaxation of the intermediate excited state have very low energy (about 540 eV, due to screening effects of the four electrons). Since the detector efficiency for these low

energy x rays is only about[32] 3% most of them are not detected. Figure 28b shows a time spectrum for x rays coincident with capture (TAC) for 12 MeV O^{6+} + He collisions at 80 mTorr gas cell pressure. Here, real coincidences are observed. This is mostly due to the fact that the x rays resulting from the relaxation of the intermediate excited state have higher energy (about 630 eV), since only three electrons screen the nuclear charge, than the x rays associated with incident O^{5+}. For incident O^{6+}, the detector efficiency is about 7%.[32]

Figure 29 presents the coincidence and total K x-ray production cross sections for O^{6+} + He. No resonant behavior was observed and the cross sections for capture and simultaneous emission of a K x-ray are seen to decrease monotonically as the projectile energy increases, a feature that is characteristic of total electron capture cross sections. We note that incident O^{6+} likely has a significant metastable fraction, i.e., O^{6+} (1s2s). Thus x-ray events coincident with capture can result when electrons are captured into shells with $n > 1$ (i.e., an x-ray is emitted during the $n=2 \rightarrow 1$ decay of the captured electron).

It can also be seen that the total K x-ray production cross sections are significantly larger than the coincidence cross sections indicating that K-shell excitation, not capture, is the dominant process leading to K x-ray emission for these O^{6+} + He collisions. The difference

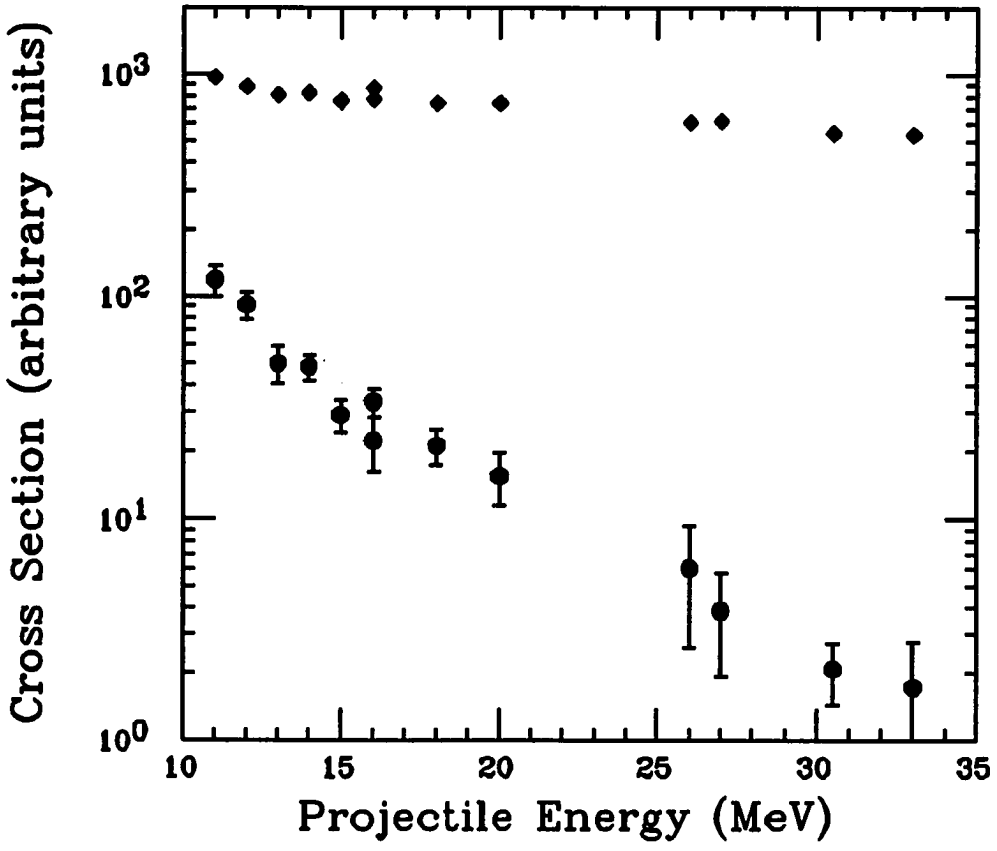

Figure 29. Coincidences (Circles) and Total X-Ray Production (Diamonds) Cross Sections Versus Projectile Energy for O^{6+} + He.

between the coincidence and the total K x-ray cross sections is seen to increase as the projectile energy increases, indicating that electron capture becomes relatively less important in x-ray production at high energies.

Cross sections for total single-electron capture were also measured in this work. Figure 30 shows a plot of the total single-electron capture cross sections, in reduced

units, for O^{6+} ions incident on He targets. The reduced electron-capture cross sections and the reduced projectile energies are given respectively by[33]

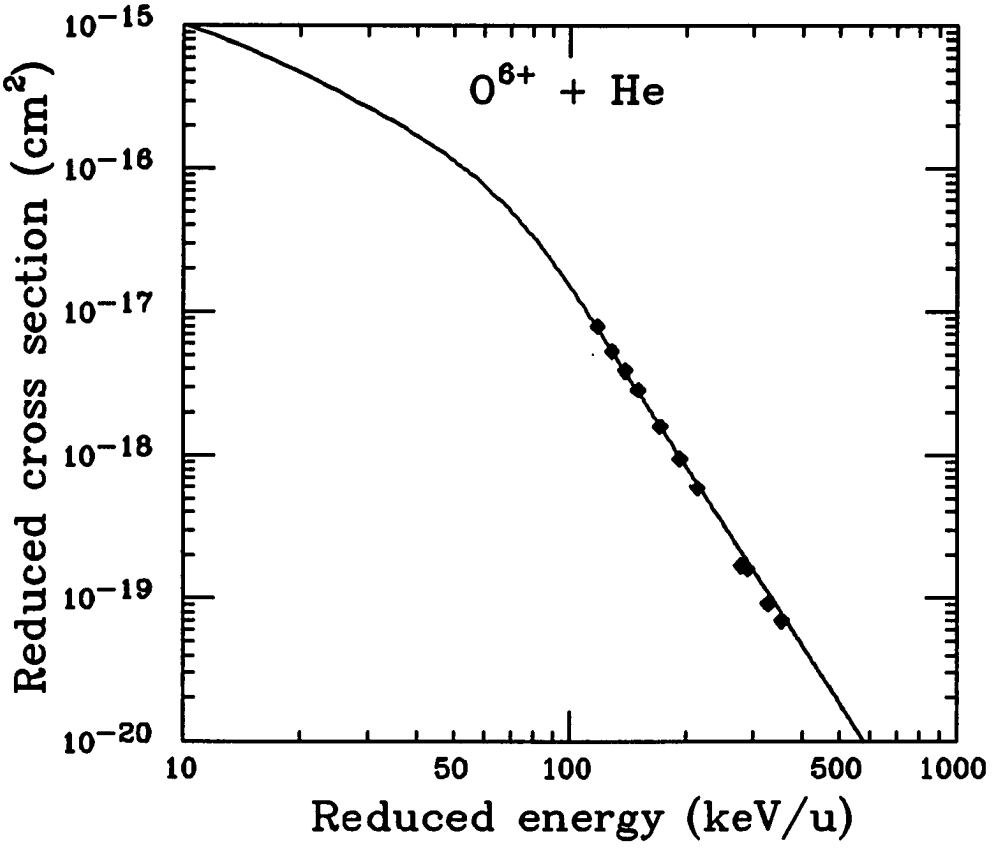

Figure 30. Reduced Plot of the Single-Electron Capture Cross Sections for O^{6+} Ions Incident on He.

The solid curve is the empirical curve of Schlachter et al., 1987.

$$\tilde{\sigma} = \sigma\left[\frac{(Z^{1.8})}{(q^{0.7})}\right] \qquad (4.19)$$

$$\tilde{E} = \frac{E}{(Z^{1.25}.q^{0.5})} \qquad (4.20)$$

where σ is the measured single-electron capture cross section, Z is the atomic number of the target, q is the charge state of the projectile ion, and E is the projectile energy (keV/u). The empirical prediction[33] for the measured cross sections is also shown in Figure 30. From the figure we see that the measured electron-capture cross sections are in good agreement with the empirical predictions.

Figure 31 shows the single-electron-capture cross sections for O^{6+} + He as a function of the beam energy. The line is a fit to the function $\sigma=\sigma_0 E^{-n}$ which gives n=4.3±0.1. This value of n is consistent with the empirical prediction[33]. The same Figure also shows the energy dependence of the cross sections for single-electron capture coincident with x-ray emission for O^{6+}+ He. The line is a fit to the function $\sigma=\sigma_0 E^{-n}$ which gives n=3.8±0.3. For both cases, the functions were derived by doing a fit to the data points. The two functions indicate that the energy dependence for the coincidence cross sections is slightly different than the energy dependence associated with capture. In fact, the total single-electron-capture cross sections decrease faster than the coincidence cross sections, as the projectile energy increases. This observation is consistent with the fact that the coincidence cross sections depend on both the capture probability and the K-shell excitation cross section (the latter cross sections decrease more slowly for the energies investigated here)

see Figure 4. This indicates that a mechanism other than capture is responsible for some of the capture-x-ray coincidences (possibly RTE or NTE).

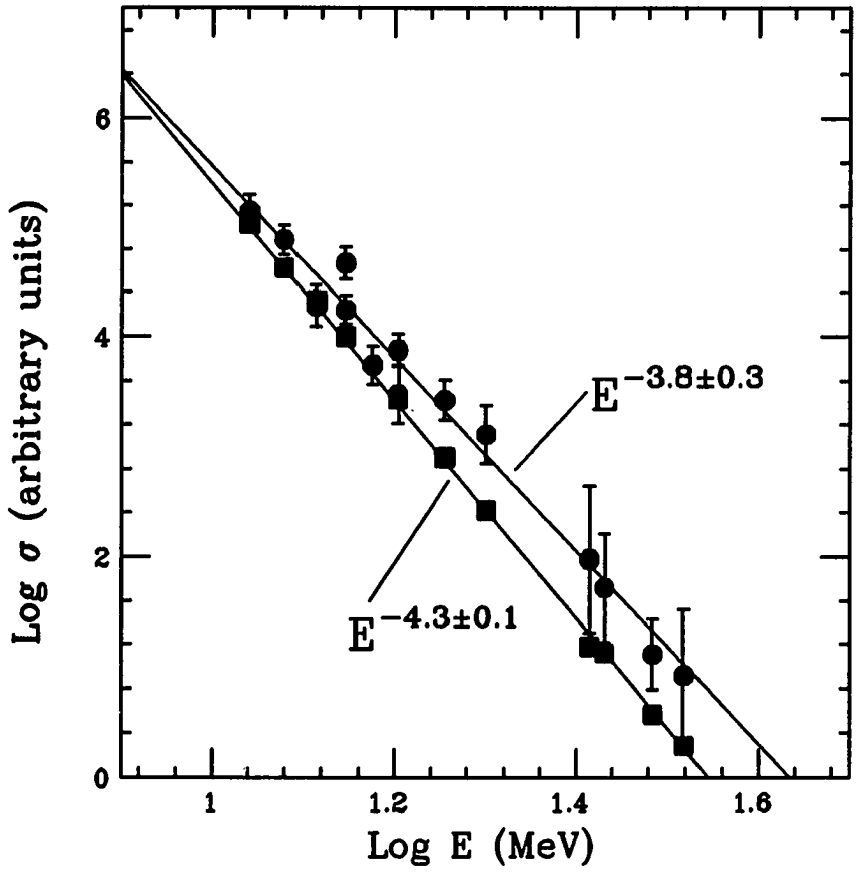

Figure 31. Single-Electron-Capture Cross Sections (Squares) for O^{6+} + He as a Function of the Beam Energy.

The line is a fit to the function $\sigma=\sigma_0 E^{-n}$ which gives n=4.3±0.1. Cross sections for single electron capture coincident with x-ray emission (circles) for the same collision system. The line is a fit to the function $\sigma=\sigma_0 E^{-n}$ which gives n=3.8±0.3.

CHAPTER V

CONCLUSIONS

Recombination has been investigated in high-energy Kr^{34+} + H_2 and O^{6+} + He collisions. Three recombination mechanisms are considered, namely, resonant transfer excitation (RTE), resonant transfer double excitation (RT2E), and radiative electron capture (REC).

For the Kr^{34+} measurements, Kr K x rays associated with RTE involving KLL transitions are readily observed and the measured cross sections are in good agreement with theory. Higher-energy x rays associated with single-electron capture are attributed to REC, and there is reasonable overall agreement with theory, but there seems to be a systematic discrepancy at the lower beam energies. No evidence for the RT2E mechanism is observed, however, in these measurements. Although this mechanism probably occurs, its estimated cross section ($< 10^{-27}$ cm^2) is too small to be measured within the sensitivity ($\sim 10^{-25}$ cm^2) of the present measurements.

In the case of O^{6+} + He, real coincidences were observed in the expected energy region for RT2E but no resonant behavior was associated with them because of the presence of metastable states, i.e., O^{6+} (1s2s), in the

incident beam which can lead to K x-ray emission following capture to the L-shell without accompanying excitation. These cross sections were found to decrease monotonically as the projectile energy increases, a feature that is characteristic of total single capture cross sections. However, least squares fits to both the coincidence and the total capture cross sections indicate that the energy dependence of the coincidence cross sections is slightly different than the energy dependence associated with capture. This indicates that a mechanism other than simple capture may be responsible for some of the coincidences (possibly RTE or NTE).

REFERENCES

1. J. B. Hasted (1972). Physics of Atomic Collisions (2nd ed.) New York: Elsevier.

2. P. L. Pepmiller, (1983). Formation of doubly excited two electron ions during F^{8+} + He, Ne, or Ar collisions. Doctoral dissertation, Kansas State University, Manhattan, KS.

3. P. L. Pepmiller, P. Richard, J. Newcomb, J. Hall, and T. R. Dillingram, Phys. Rev., A31, 734 (1985)

4. For a review, see J. A. Tanis, Recombination of Atomic Ions, edited by W. G. Graham, W. Fritsch, Y. Hahn, and J. A. Tanis, (Plenum, New York, 1992), pp. 241-257.

5. M. Schulz, R. Schuch, S. Datz, E. L. B. Justiniano, P. D. Miller, and H. Schone, Phys. Rev., A38, 5454 (1988).

6. M. J. Seaton, and P. J. Storey (1976). Dielectronic recombination. In P. G. Burke and B. L. Moiseiwitsch (Eds.), Atomic processes and applications (pp. 133-197). New York: North Holland Publishing.

7. A. Burgess, Astrophysical Journal, 139, 776 (1964).

8. A. L. Merts, R. D. Cowan, and N. H. Magee Jr., Los Alamos Scientific Laboratory Informal Report, LA-62200-MS, 1976.

9. N. R. Badnell, private communication, 1991.

10. A. Müller, G. Hofmann, B. Weissbecker, M. Stenke, K. Tinschert, M. Wagner, and E. Salzborn, Phys. Rev. Lett., 63, 7 (1989).

11. V. V. Afrosimov, Yu. S. Gordeev, A. N. Zinov'ev, D. Kh. Rasulov, and A. P. Shergin, Sov. Phys. JETP Lett., 21, 249 (1975).

12. W. Wolfli, Ch. Stoller, G. Bonani, M. Suter, and M. Stöckli, Phy Rev. Lett., 35, 656 (1975).

13. W. Heisenberg, Z. Phys., 32, 841 (1925).

14. H. W. Schnopper, Hans D. Betz, J. P. Delvaille, K. Kalata, A. R. Sohval, K. W. Jones, and H. E. Wegner, Phys. Rev. Lett., 29, 898 (1972).

15. See Y. Hahn and K. J. LaGattuta, Phys. Rep. 166, 196 (1988), and references therein.

16. See M. H. Chen, Recombination of Atomic Ions, edited by W. G. Graham, W. Fritsch, Y. Hahn, and J. A. Tanis, (plenum, New York, 1992), pp. 61-76 and references therein.

17. M. S. Pindzola, N. R. Badnell, and D. C. Griffin, ibid, pp. 99-106, and references therein.

18. J. M. Feagin, J. S. Briggs, T. M. Reeves, (1984). Simultaneous charge transfer and excitation. Journal of Physics, B17, 1057-1068.

19. J. A. Tanis, E. M. Bernstein, M. W. Clark, W. G. Graham, R. H. McFarland, T. J. Morgan, B. M. Johnson, K. W. Jones, and M. Meron (1985). Evidence for uncorrelated electron capture and K-shell excitation in S^{13+} + He collisions. Physical Review, A31, 4040-4042.

20. T. M. Reeves, J. M. Feagin, and E. Merzbacher, 14th International Conference on the Physics of Electronic and Atomic Collisions, Palo Alto, California, 1985, Abstracts of Contributed Papers, M. J. Coggiola, D. L. Huestis, and R. P. Saxon, eds., p. 392.

21. J. K. Swenson, Y. Yamazaki, P. D. Miller, H. F. Krause, P. F. Dittner, P. L. Pepmiller, S. Datz, and N. Stolterfoht (1986). Observation of Resonant Transfer and Excitation to Specific LS-Coupled states in O^{5+} + He Collisions by High-Resolution, 0^0 Auger-Electron Spectroscopy. Physical Review Letters, 57, 3042-3045.

22. A. K. Bhatia, and A. Temkin, (1977). A distorted-wave methodology for electron-ion impact excitation: Calculation for two-electron ions. Journal of Physics, B10, 2893-2912.

23. D. Brandt, Phys. Rev., A27, 1314 (1983).

24. F. Biggs, L. B. Mendelson, and J. B. Mann, (1975). Hartree-Fock Compton profiles for the elements. Atomic Data and Nuclear Data Tables, 16, 201-309.

25. I. P. Grant, Advances in Physics, 19, 747 (1970)

26. H. E. Bethe and E. E. Salpeter, Quantum Mechanics of One-and Two-Electron Atoms (Academic, New York, 1957), pp. 320-322.

27. M. Kleber and D. H. Jakubassa, Nucl. Phys. A252, 152 (1975).

28. For a discussion of the energy degrader and the A1200 analysis device, see, for example, NSCL Newletter, NSCL-N12, April 1991, Michigan State University.

29. G. W. F. Drake, Phys. Rev. A3, 908 (1971).

30. N. R. Badnell, private communication, 1995.

31. Th. Stöhlker, Ph.D. Thesis, University of Giessen, Germany, 1991 (unpublished).

32. Selection Guide and Price List for Solid-State Photon Detectors and Accessories, January 1982, EG&G ORTEC Nuclear Technology Division, 100 Midland Road, Oak Ridge, Tennessee 37830.

33. Schlachter A. S., Stearns, J. W., Berker, K.H., Stockli, M. P., Graham, W. G., Bernstein, E. M., Clark, M. W., and Tanis, J. A., Abstracts of Contributed Papers, Proceedings of the Fifteenth International Conference of the Physics of Electronic and Atomic Collisions, Brighton, United Kingdom, 1987, edited by Gedes, J., Gilbody, H. B., Kingston, A. E., Latimer, C. J., and Walters, H. J. R. (Queens University, Belfast, 1987), 505.

BIBLIOGRAPHY

Afrosimov, V. V., Gordeev, Yu.S., Zinov'ev, A. N., Rasulov, D. Kh., and Shergin, A. P., Sov. Phys. JETP Lett., 21, 249 (1975).

Badnell, N. R., private communication, 1991.

Badnell, N. R., private communication, 1995.

Bethe, H. E., and Salpeter, E. E., Quantum Mechanics of One-and Two-Electron Atoms (Academic, New York, 1957), pp. 320-322.

Bhatia, A. K., and Temkin, A., (1977). A distorted-wave methodology for electron-ion impact excitation: Calculation for two-electron ions. Journal of Physics, B10, 2893-2912.

Biggs, F., Mendelson, L. B., and Mann, J. B. (1975). Hartree-Fock Compton profiles for the elements. Atomic Data and Nuclear Data Tables, 16, 201-309.

Brandt, D. Phys. Rev., A27, 1314 (1983).

Burgess, A. Astrophysical Journal, 139, 776 (1964).

Chen, M. H. Recombination of Atomic Ions, edited by W. G. Graham, W. Fritsch, Y. Hahn, and J. A. Tanis, (plenum, New York, 1992), pp. 61-76 and references therein.

Drake, G. W. F., Phys. Rev. A3, 908 (1971).

Feagin, J. M., Briggs, J. S., Reeves, T. M. (1984). Simultaneous charge transfer and excitation. Journal of Physics, B17, 1057-1068.

Grant, I. P., Advances in Physics, 19, 747 (1970)

Hahn, Y., and LaGattuta, K. J., Phys. Rep. 166, 196 (1988), and references therein.

Hasted, J. B. (1972). Physics of Atomic Collisions (2nd ed.) New York: Elsevier.

Heisenberg, W., Z. Phys., 32, 841 (1925).

Kleber M., and Jakubassa, D. H., Nucl. Phys. A252, 152 (1975).

Merts, A. L., Cowan, R. D., and Magee Jr., N. H., Los Alamos Scientific Laboratory Informal Report, LA-62200-MS, 1976.

Müller, A., Hofmann, G., Weissbecker, B., Stenke, M., Tinschert, K., Wagner, M., and Salzborn, E. Phys. Rev. Lett., 63, 7 (1989).

Pepmiller, P. L. (1983). Formation of doubly excited two electron ions during F^{6+} + He, Ne, or Ar collisions. Doctoral dissertation, Kansas State University, Manhattan, KS.

Pepmiller, P. L., Richard, P., Newcomb, J., Hall, J., and Dillingram, T. R., Phys. Rev., A31, 734 (1985)

Pindzola, M. S., Badnell, N. R., and Griffin, D. C., ibid, pp. 99-106, and references therein.

Reeves, T. M., Feagin, J. M., and Merzbacher, E. 14th International Conference on the Physics of Electronic and Atomic Collisions, Palo Alto, California, 1985, Abstracts of Contributed Papers, M. J. Coggiola, D. L. Huestis, and R. P. Saxon, eds., p. 392.

Schlachter A. S., Stearns, J. W., Berker, K.H., Stockli, M. P., Graham, W. G., Bernstein, E. M., Clark, M. W., and Tanis, J. A., Abstracts of Contributed Papers, Proceed ings of the Fifteenth International Conference of the Physics of Electronic and Atomic Collisions, Brighton, United Kingdom, 1987, edited by Gedes, J., Gilbody, H. B., Kingston, A. E., Latimer, C. J., and Walters, H. J. R. (Queens University, Belfast, 1987), 505.

Schnopper, H. W., Hans D. Betz, Delvaille, J. P., Kalata, K., Sohval, A. R., Jones, K. W., and Wegner, H. E. Phys. Rev. Lett., 29, 898 (1972).

Schulz, M., Schuch, R., Datz, S., Justiniano, E. L. B., Miller, P. D., and H. Schone, Phys. Rev., A38, 5454 (1988).

Seaton, M. J., and Storey P. J. (1976). Dielectronic recombination. In P. G. Burke and B. L. Moiseiwitsch (Eds.), Atomic processes and applications (pp. 133-197). New York: North Holland Publishing.

Stöhlker, Th., Ph.D. Thesis, University of Giessen, Germany, 1991 (unpublished).

Swenson, J. K., Yamazaki, Y., Miller, P. D., Krause, H. F., Dittner, P. F., Pepmiller, P. L., Datz, S., and Stolterfoht N. (1986). Observation of Resonant Transfer and Excitation to Specific LS-Coupled states in O^{5+} + He Collisions by High-Resolution, 0^0 Auger-Electron Spectroscopy. Physical Review Letters, 57, 3042-3045.

Tanis, J. A., Recombination of Atomic Ions, edited by W. G. Graham, W. Fritsch, Y. Hahn, and J. A. Tanis, (Plenum, New York, 1992), pp. 241-257.

Tanis, J. A., Bernstein, E. M., Clark, M. W., Graham, W. G., McFarland, R. H., Morgan, T. J., Johnson, B. M., Jones, K. W., and Meron M. (1985). Evidence for uncorrelated electron capture and K-shell excitation in S^{13+} + He collisions. Physical Review, A31, 4040-4042.

Wolfli, W., Stoller, Ch., Bonani, G., Suter, M., and Stöckli, M. Phy Rev. Lett., 35, 656 (1975).